

Aus der Medizinischen Klinik mit Schwerpunkt Infektiologie und  
Pneumologie  
der Medizinischen Fakultät Charité – Universitätsmedizin Berlin

## **DISSERTATION**

### **Novel biomedical applications for spectrally resolved fluorescence lifetime imaging microscopy**

Doctor rerum medicinalium (Dr. rer. medic.)

vorgelegt der Medizinischen Fakultät  
Charité – Universitätsmedizin Berlin

von

Sumeet Rohilla

aus Chennai, India

Datum der Promotion: 05. 03. 2021



# Contents

---

<b>Abstract (English)</b> .....	IV
<b>Abstract (Deutsch)</b> .....	V
<b>1. Introduction</b> .....	1
<b>2. Materials and Methods</b>	
2.1 Antibodies.....	5
2.2 Sample preparation.....	5
2.3 sFLIM experimental setup.....	6
2.4 Fluorescence lifetime analysis.....	8
2.5 Generation of reference patterns.....	9
2.6 Bleed-through calculation.....	9
2.7 Statistical analysis.....	9
2.8 Data and code availability.....	10
<b>3. Results</b>	
3.1 Paper I: Multi-target immunolabelling using cross-labelling antibodies.....	11
3.2 Paper II: Rapid-sFLIM enables high throughput imaging.....	16
3.3 Outlook: Multi-target sFLIM imaging of human lung tissue samples.....	18
<b>4. Discussion and Conclusion</b> .....	22
<b>5. Bibliography</b> .....	26
<b>6. Contributions by Author</b> .....	29
<b>7. Statutory Declarations</b> .....	30
<b>8. Publications</b> .....	32
<b>9. Curriculum Vitae</b> .....	53
<b>10. List of Publications</b> .....	54
<b>11. Acknowledgements</b> .....	55

## List of Figures

---

- Figure 1 Cross-labelling scenarios in multi-target studies.
- Figure 2 sFLIM experimental setup and pattern-matching analysis
- Figure 3 Cross-labelling antibodies undergo FLIM-FRET
- Figure 4 Labelling procedure for triple antigen IMF in cells
- Figure 5 sFLIM analysis of triple-labelled cells
- Figure 6 rapid-sFLIM enables data acquisition at high throughput
- Figure 7 Lung tissue autofluorescence characterization
- Figure 8 Multi-target IMF labelling of highly autofluorescent lung tissue samples

## List of Tables

---

- Table 1 Fluorescence lifetime values of fluorophore-tagged secondary antibodies
- Table 2 Fluorescence lifetime values of triple immunolabelled cells
- Table 3 Bleed-through calculations



## Acronyms

---

FRET	Förster resonance energy transfer
sFLIM	Spectrally-resolved fluorescence lifetime imaging
MSI	Multi-spectral imaging
IMF	Indirect immunofluorescence
ABs	Antibodies
SNR	Signal-to-noise ratio
AF	Autofluorescence
TCSPC	Time-correlated single photon counting
PIE	Pulsed interleaved excitation
GaAsP	Gallium arsenide phosphide
TTTR	Time-tagged time-resolved
PMT	Photomultiplier tube
IRF	Instrument response function
RBCs	Red blood cells
AM	Alveolar macrophages
EMP	Extra-cellular matrix protein
proSP-C	Prosurfactant protein C
CD68	Cluster of differentiation 68

## ABSTRACT

---

Indirect labelling techniques of biomolecules with primary and secondary antibodies for immunofluorescence-based imaging is still serving well the needs of biologists in advancing the understanding of biological processes. However, these techniques impose a stringent selection of primary and secondary antibody pairs to avoid false-positive cross-labelling leading to misinterpretation, in particular for (co-)localization / interaction of target molecules. Due to this, indirect immunofluorescence is either regularly limited to two - four antigens or a particular combination of target molecule labelling can't be carried out at all. This work presents a novel immunolabelling method to use this ostensible disadvantage of cross-labelling secondary antibodies for separation of their fluorescence signals from single labelled structures by use of multi-dimensional fluorescence detection. This becomes possible since the undesirable cross-labelling among secondary antibodies leads to the generation of new characteristic Förster resonance energy transfer (FRET) emission spectra as well as change in fluorophores lifetime properties. To demonstrate this, a sequential antibody labelling protocol was adapted and appropriate fluorophore pairs were selected on interacting secondary antibodies achieving FRET effects. A spectrally resolved fluorescence lifetime imaging (sFLIM) system and multi-wavelength pulse interleaved excitation were combined together for multi-dimensional signal detection. The short dead time of the time-correlated single photon counting electronics allows for rapid-sFLIM measurements enabling data acquisition at very high detection throughput. For data analysis, a pattern-matching based linear-unmixing technique was employed for efficient identification and unmixing of multi-labelled samples using reference emission spectra and fluorescence decay patterns from each immunolabelled biomolecule. Additionally, separation of up to three immunolabelled proteins from strong autofluorescence components in human lung tissue sections by sFLIM detection and applying appropriate autofluorescence reference patterns in unmixing analysis was demonstrated. The spectral-FLIM(-FRET) detection system together with pattern-matching analysis forms an excellent tool for use in indirect immunofluorescence by overcoming the undesirable effect of secondary antibody cross-labelling by assigning separate colour channels to cross-labelled antigens or proteins. Altogether, this work demonstrates that spectral-FLIM could greatly enhance sensing and unmixing capabilities for native autofluorescence and/or external fluorescent markers in biomedical as well as clinical research.

# ZUSAMMENFASSUNG

---

Im Bereich der Immunfluoreszenz-basierten Bildgebung sind indirekte Markierungstechniken von Biomolekülen mit primären oder sekundären Antikörpern von großem Wert, um das Verständnis biologischer Prozesse zu vertiefen. Um falsch-positive Kreuzreaktionen zu vermeiden, gelten jedoch stringente Auswahlkriterien an Primär- und Sekundärantikörperpaare. Solche Kreuzreaktionen können zu Fehlinterpretationen führen, insbesondere in den Bereichen (Co-) Lokalisierung und Wechselwirkung der Zielmoleküle. Dies hat wiederum zur Folge, dass indirekte Immunfluoreszenz häufig auf zwei-vier Antigene beschränkt ist oder dass bestimmte Markierungskombinationen gar nicht möglich sind. In dieser Dissertation wird eine neuartige Methode zur Immunmarkierung vorgestellt, welche die offensichtlichen Nachteile der Kreuzreaktion von sekundären Antikörpern ausnutzt, um die Fluoreszenzsignale einfach markierter Strukturen mittels multidimensionaler Fluoreszenzdetektion zu unterscheiden. Die Methode basiert darauf, dass die unerwünschte Kreuzreaktion zwischen sekundären Antikörpern sowohl zum Auftreten neuer, spezifischer Fluoreszenzenergietransfers-Emissionsspektren (FRET) als auch zu Veränderungen in den Fluoreszenzlebensdauern der Fluorophore führt. Um dies zu demonstrieren, haben wir ein sequentielles Antikörpermarkierungsprotokoll entworfen und entsprechende Fluorophorpaare für interagierende sekundäre Antikörper identifiziert, unter welchen FRET möglich ist. Für die Detektion wurde ein spektral- und zeitauflösendes Fluoreszenzlebensdauersystem (sFLIM) genutzt, welches über ein verschachtelt-gepulstes Anregungssystem mit multiplen Wellenlängen sowie über ein multidimensionales Detektionssystem verfügt. Dank der kurzen Totzeit der eingesetzten Elektronik für die zeitkorrelierte Einzelphotonenzählung können sogenannte rapid-sFLIM Messungen mit sehr hohem Detektionsdatendurchsatz durchgeführt werden. In der Datenanalyse wurde eine Technik zum Musterabgleich angewandt, die eine effiziente Identifikation und Entmischung von mehrfach markierten Proben mittels Referenzemissionsspektren sowie Fluoreszenzabklingmustern der jeweiligen immun-markierten Biomoleküle erlaubt. Zusätzlich demonstriert die Arbeit die Abtrennung der Fluoreszenzsignale von bis zu vier immun-markierten Proteinen sowie der Hintergrundautofluoreszenz von menschlichem Lungengewebe mittels sFLIM Detektion durch Anwendung passender Referenzmuster im Entmischungs- und Analyseschritt. Die Kombination eines spektralen FLIM-(FRET) Detektionssystems mit einer Musterabgleichsanalyse erweist sich als ein sehr nützliches

Werkzeug für indirekte Immunofluoreszenz Untersuchungen. Sie überwindet die unerwünschten Nebeneffekte der Kreuzreaktion von sekundären Antikörpern indem sie kreuzreagierende Antigene oder Proteinen jeweils in einen separaten Farbkanal zuweist. Insgesamt wird in dieser Arbeit aufgezeigt, dass die simultane Detektion von Fluoreszenzabklingzeiten und Charakteristika von Emissionsspektren mittels spektral-FLIM, die Empfindlichkeit und Separierung der einzelnen Komponenten signifikant verbessern kann. Dies gilt sowohl für native Autofluoreszenz wie auch für externe Fluoreszenzmarker in der biomedizinischen oder klinischen Forschung.

# 1. INTRODUCTION

---

Fluorescence microscopy has become a pivotal technique in modern day biological research for the detection and visualization of specific proteins in fixed and living cells as well as tissue sections and microarrays<sup>1</sup>. Recent trends in biomedical and clinical research suggests that simultaneous detection of larger numbers of biomarkers allow for a more precise diagnosis, thereby improving treatment success rate<sup>2-4</sup>. Consequently, monitoring the expression of different target molecules via microscopic imaging is becoming increasingly important, even crucial, for basic biomedical and clinical research purposes<sup>5</sup>.

To date, indirect immunofluorescence (IMF) labelling of target biomolecules with primary and fluorophore-tagged secondary antibodies (ABs) is still one of the most extensively used methods because it allows for selective and specific detection of biomarkers with high signal-to-noise ratios (SNR)<sup>6-8</sup>. However, adapting IMF methods for labelling of multiple antigens requires careful selection of primary and corresponding secondary antibodies (ABs) to avoid false-positive detection due to host animal species overlap<sup>9,10</sup>. Another crucial aspect of IMF is the meticulous need for AB specificity validation using single label controls and that it must be retained when multiple ABs are used in single sample staining protocols. Typically, primary ABs originating from different host species are combined with secondary ABs, all raised in one disparate host species, or at least differing from the species origin of all primary and other secondary ABs (Fig. 1A). Even though a broad host species panel of primary ABs is principally available (e.g. mouse, human, rabbit, rat, goat, chicken, sheep, guinea pig, hamster, bovine, donkey, dog, camelid, cat, pig etc.), in practice, most well-performing and specific primary ABs for important target antigens originate from mouse, rabbit, rat or goat. This limits the number of target molecules that can be labelled and detected simultaneously in a single experiment due to AB species overlap. A series of solutions have been proposed by researchers to avoid double immunolabelling artefacts due to ABs raised in same host species<sup>11-17</sup>, but these still do not completely tackle the problem of false-positive cross-labelling, and therefore bear the risk of misinterpretation regarding spatial co-localization distribution, or even interaction of molecules<sup>18-20</sup>. Additionally, these techniques require the use of chemical reagents, increased sample preparation time and sophisticated analysis, all of which hinder their practical use in many research laboratories. Another challenge of multi-target fluorescence microscopy of tissue sample is that the intrinsic

autofluorescence (AF) emission frequently invades the spectral emission of commonly used fluorophore-tagged ABs and hampers the quantitation analysis for estimation of co-expression and co-localization of multiple biomarkers<sup>21-23</sup> (Fig. 1B). Limitations such as these highlight the need for developing innovative AB multiplexing protocols together with multi-dimensional fluorescence imaging systems and analysis methods demonstrating faster and simultaneous acquisition of multiple fluorophore-tagged biomolecules and subsequent suppression of background sample AF.

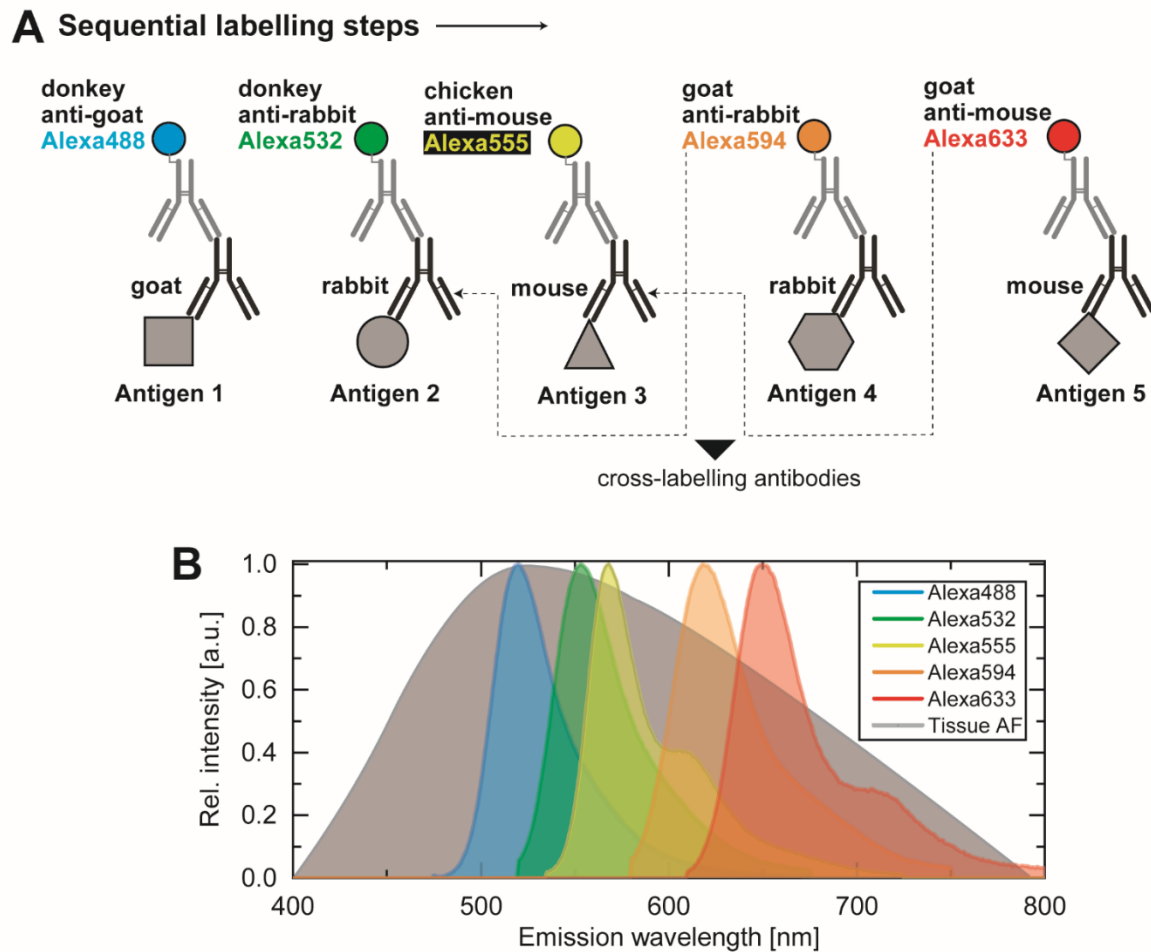


**Figure 1:** A typical sequential labelling procedure used for indirect immunofluorescence (IMF) of five target antigens to demonstrate the resulting cross-labelling scenarios in multi-target studies. **(A)** Primary antibodies (ABs) originating from goat, rabbit and mouse bind to antigen 1, 2 and 3, respectively. For IMF detection, fluorophore-tagged secondary ABs (“donkey-anti-goat Alexa488”, “donkey-anti-rabbit Alexa532” and “chicken-anti-mouse Alexa555”), all having different origins than primary ABs, will not show any cross-labelling thus far. However, well-performing primary antibodies for target antigen 4 and 5 originate from rabbit and mouse, and subsequent IMF labelling steps with secondary ABs (“goat-anti-rabbit Alexa594” and “goat-anti-mouse Alexa633”) will lead to cross-labelling of rabbit and mouse primary AB for antigen 2 and antigen 3 with “goat-anti-rabbit Alexa594” and “goat-anti-mouse Alexa633”, raising the risk of misinterpretation of results such as false-positive co-localization or even antigen-antigen interaction. **(B)** Autofluorescence (AF) emission of a tissue sample often covers the entire spectral detection range of commonly used fluorophores in multi-target studies. The highly intense native tissue AF (grey line) often bleeds into the detection

channels of each fluorophore labelling, hindering their precise identification and separation. Multi-dimensional detection systems could potentially provide better separation due to simultaneous detection of characteristic fluorescence signatures from single- and cross-labelled species in autofluorescent cell or tissue samples.

In **Paper I**, a novel IMF labelling procedure is proposed that transforms this undesired cross-labelling AB effect into an advantage by appropriately attributing new independent fluorescence analysis channels<sup>24</sup>. A necessary and sufficient condition for achieving this advantage is that single- as well as cross-labelled structures exhibit significant differences in their fluorescence signatures allowing for unambiguous separation and channel specific signal attribution. Selecting interacting fluorophores on the closely bound cross-labelling ABs such that there is considerable overlap between their absorption and emission spectra, will lead to change in their chemical-physical properties through the “Förster resonance energy transfer (FRET)” phenomenon, which was already shown by previous work of Holzapfel *et al.*<sup>25</sup>. When a pair of fluorophores, also called a donor / acceptor pair, on cross-labelled ABs are in close proximity to one another ( $< 10$  nm), FRET occurs via radiation-less transfer of energy from donor to acceptor molecule<sup>26</sup>. FRET interactions result in shifts in two important fluorescence characteristics: (1) a decrease in donor intensity and concomitant increase in acceptor intensity leading to change in donor / acceptor emission spectra profile, (2) a decrease in donor fluorophore lifetime leading to change in its observed fluorescence lifetime decay shape. Therefore, simultaneous detection of emission spectra as well as nanosecond fluorescence lifetime decay makes it possible to separate cross-labelled species from single-labelled target biomolecules. To proof this hypothesis, we adapted a sequential IMF labelling procedure on A549 cells and selected appropriate FRET compatible fluorophores on cross-labelling ABs, thereby achieving triple antigen labelling using just two fluorophores. Furthermore, simultaneous acquisition of emission spectra and fluorescence lifetime decay is accomplished by means of time-domain spectrally resolved fluorescence lifetime imaging (spectral-FLIM or sFLIM)<sup>27-29</sup>. The combination of two non-filter-based confocal imaging modalities, multi-spectral imaging and time-resolved FLIM, allows for quantification of FRET effects with high precision and single molecule sensitivity as well as separation of up to nine different fluorophores in the cellular environment<sup>27,30-34</sup>. In this view, we built an 8-channel sFLIM system for quantification and verification of FRET signatures resulting from interaction of fluorophores on secondary ABs as well as an already established linear-unmixing-based

pattern-matching algorithm<sup>27</sup> to precisely separate cross- and single-labelled target molecules in a typical biological multiplexed IMF scenario. The pattern-matching algorithm achieves optimal unmixing results by combining emission spectra as well as fluorescence decay information.

The combination of multi-spectral imaging and FLIM has shown potential in biological studies, for instance in histopathology as well as in the cancer research field<sup>23,35</sup>. However, the true potential of sFLIM system still remains unexploited due to long dead times of photon detection electronics, which result in slow data acquisition speeds. To overcome this limitation, PicoQuant GmbH developed a fast time-correlated single photon counting (TCSPC) device with ultra-short dead times maintaining good temporal resolution. In **Paper II**, using this fast detection system (henceforth called rapid-sFLIM), we present an exemplary life science application, which provides faster data acquisition speeds due to the instrument's capability to operate at high sustained data throughput independently in all channels<sup>36</sup>. Finally, as an outlook, we present a representative application of a rapid-sFLIM imaging technique for multi-target fluorescence imaging of highly autofluorescent human lung tissue samples. First, using the rapid-sFLIM imaging system, we could demonstrate that fluorescence lifetime provides a better contrast mechanism compared to multi-spectral imaging, which was then employed to develop a reliable and systematic method for discrimination of endogenous fluorophores with overlapping spectra. Second, we demonstrate how multiplexing in standard as well as advanced IMF becomes possible with cross-labelling ABs. With the results from these proof-of-concept studies, we expand the toolbox of IMF and demonstrate potential applicative benefits of the multi-dimensional (rapid-) sFLIM imaging method in tackling challenges in modern-day biomedical as well as clinical research.

Note to Readers: A large part of the results presented in the following sections have been published in journal articles<sup>24,36</sup>. Here, I present a summary of that work using references to the figures in journal articles. For in-depth description of analysis and results, the reader is requested to take a deeper look at the original journal articles. Additionally, I present some data and results which are unpublished and form an outlook part of this dissertation work (Fig.7-8 and Table 3).



## 2. MATERIALS AND METHODS

---

### 2.1 Antibodies

The primary ABs against pan-cytokeratin and TOM20 were obtained from Santa Cruz Biotech (Germany). The anti-golgin primary AB and the Alexa Fluor® conjugated secondary AB were purchased from ThermoFisher Scientific (Germany). The “unconjugated rabbit-anti-mouse” and “unconjugated goat-anti-rabbit” secondary ABs were from Dianova (Germany).

The primary ABs against EMP (extra-cellular matrix protein), proSPC (surfactant protein C) and CD68 protein (cluster of differentiation protein 68) were purchased from Atlas-Antibodies (Germany), abcam (Germany), and MilliporeSigma (USA), respectively.

### 2.2 Sample preparation

**Cell cultures and indirect immunofluorescence labelling.** Human lung alveolar epithelial cell line A549 (ATCC, CCL-185) was cultured in Ham's F12 medium (Biochrome, Berlin, Germany) supplemented with 10% fetal calf serum at 37°C and 5% CO<sub>2</sub>. Cells were seeded on optical coverslips. After three washes with phosphate buffered saline (PBS), cells were fixed with 3% paraformaldehyde for 15 min at room temperature followed by three washes with PBS. Afterwards, cells were permeabilized with 1.0% Triton X-100 for 15 min. After washing with PBS, cells were blocked with AB diluent (20 ml PBS 0.01 M with 0.2 g BSA and 0.01 g Tween-20) and primary ABs (2 µg/ml) were incubated overnight at 4°C. After three washes with PBS, cells were subjected to an overnight incubation with respective secondary AB at 4°C. Immunolabelled cells were embedded in MOWIOL for 20 min at 4°C.

For triple antigen IMF of A549 cells, sequential labelling was performed to achieve single labelling of TOM20 with “goat-anti-rabbit Alexa488” and golgin with “rabbit-anti-mouse Alexa546”, as well as cross-labelling of pan-cytokeratin with “rabbit-anti-mouse Alexa546” and “goat-anti-rabbit Alexa488”. In a similar manner, as described above, a zero FRET control sample was also prepared for pan-cytokeratin. For optimal unmixing results, single-labelled samples for only TOM20 (with “goat-anti-rabbit”) and golgin (with “rabbit-anti-mouse Alexa546”) were prepared and imaged to obtain correct reference patterns.

**Human lung tissue and immunofluorescence labelling.** Tumour-free lung tissues were obtained from patients undergoing surgery at different medical centres in Berlin. Written informed consent was obtained from all patients, and the study was approved by the ethics committee at the Charité clinic (project EA2/079/13). To begin with, sliced sections of 3mm thickness were stamped into small cylinders (diameter 8 mm) using a biopsy punch (diameter 8 mm) and weighed. Next, to wash off the residual clinically applied antibiotics, tissue samples were incubated overnight in RPMI 1640 medium at 37 °C and 5 % CO<sub>2</sub>. The lung tissue was cut with a scalpel into slices of approximately 3 mm thickness. For deparaffinization, the tissue sections were heated at 60°C overnight and washed for 3 X 15 min with Roticlear (Roth, Karlsruhe, Germany). Thereafter, tissues were rehydrated in descending ethanol concentrations, ending in 0.01 M PBS (pH 7.6). For epitope recovery, tissue sections were incubated in Tris-EDTA buffer (1 M Tris, 0.5 M EDTA, pH 9.0) at 95 °C for 30 min. After three washes with PBS, tissues were permeabilized using 1% Triton X-100 for 15 min and washed three times again. Next, blocking was performed for 30 min with 5% goat serum and diluent (20 ml PBS 0.01 M with 0.2 g BSA and 0.01 g Tween-20). For IMF labelling, primary ABs (2 µg/ml) were incubated overnight at 4°C. After three washes with PBS, tissue sections were subjected to an overnight incubation with the respective secondary ABs at 4°C. Finally, after three washes with PBS, labelled tissues were embedded in MOWIOL for 20 min at 4°C.

For AF characterization, tissue samples were obtained from 20 different patients and similar sample preparation procedures were performed except for overnight incubation with antibody labelling.

For triple-protein IMF of tissue samples, we adapted a sequential procedure to achieve single-labelling of proSPC with “goat-anti-rabbit Alexa488” and CD68 with “goat-anti-mouse Alexa546”, as well as cross-labelling of EMP with “goat-anti-rabbit Alexa546” and “goat-anti-rabbit Alexa488”. In a similar manner, as described above for cellular labelling, a zero-FRET control sample was also prepared for EMP. For optimal unmixing results, a single stained sample for proSPC and CD68 as well as an AF slide from same patients was prepared and imaged to obtain correct reference patterns.

## **2.3 sFLIM experimental setup**

Conventional channel mode measurements were performed using a time-resolved microscope (MicroTime 200, PicoQuant, Germany) equipped with a galvo scanner

(FLIMbee, PicoQuant, Germany) and two SPAD detectors (PicoQuant, Germany) with 520/35 nm and 593/20 nm bandpass filters (AHF Analysentechnik AG, Germany). For triple antigen cellular IMF, intensities in three analysis channels corresponded to following combinations of pulsed interleaved excitation (PIE) mode and detection bandpass filters: Ch. 1 – excitation at 485 nm wavelength, detection spectral band of 520/35 nm, Ch. 2 – excitation at 485 nm wavelength, detection spectral band of 593/20 nm and Ch. 3 – excitation at 560 nm wavelength, detection spectral band of 593/20 nm. The confocal microscopy setup used for sFLIM measurements is shown in Fig. 2A<sup>24</sup>. Measurements including dye solutions and cell cultures were performed on a time-resolved microscope (MicroTime 200) equipped with a galvo scanner (FLIMbee) and an 8-channel TCSPC module (HydraHarp 400, PicoQuant, Germany) operated by the commercially available software (SymPhotime 64, PicoQuant, Germany). Human lung tissue samples were investigated using a Zeiss LSM 780 (Carl Zeiss, Germany) equipped with the sFLIM upgrade kit including an 8-channel TCSPC module enabling faster measurements over the aforementioned setup version (MultiHarp, PicoQuant, Germany). For all the measurements, linearly polarized light from pulsed laser with wavelength 485 nm and 560 nm (LDH-D-C-485 and LDH-D-TA-560, PicoQuant, Germany) operated in PIE mode was used for sample excitation. Lasers were operated at repetition frequency of 40 MHz in PIE mode with an average measured power of 3  $\mu$ W to 6  $\mu$ W after the oil-immersion objective. The custom-developed sFLIM system by PicoQuant works as an add-on to any modern-day inverted laser scanning microscope (LSM) unit. The fluorescence light emitted by the sample was guided using a multimode fibre to the sFLIM system consisting of a spectrograph, an array PMT detector and an 8-channel TCSPC unit. The fluorescence light was dispersed into its constituent spectral components with a grating-based spectrograph (Shamrock SR-163 equipped with SR1-397 GRT-0600-0500 grating, Andor Oxford Instruments, UK) and then further detected on a 16-channel PMT array (H13123-40, Hamamatsu, Germany) with gallium arsenide phosphide (GaAsP) cathodes. The PMT detection array was configured to create eight spectral channels corresponding to eight TCSPC channels. In this way, a spectral detection range of 400 nm to 640 nm was covered with each spectral channel spacing equalling 18.8 nm between successive channels. The photonic signal from each channel was further amplified by an amplifier module (PAM 102-P, PicoQuant, Germany) and connected to the timing input channel of the TCSPC unit. The signal from the multi-

spectral sFLIM system was recorded in TTTR (time-tagged time-resolved)<sup>37</sup> format comprising timing and channel information corresponding to each detected photon. The raw TTTR image files were analyzed using custom-written pattern-matching software in MATLAB (MathWorks, USA). The pattern-matching analysis was performed on 16-core CPU (Intel® Xeon® CPU E5-2680, clock speed of 2.7 GHz) and 28-core CPU (Intel® Core i9-9880XE) corresponding to cell and human lung tissue section sFLIM imaging data respectively (Fig. 2B). The use of multi-core CPUs and custom-developed batch processing software for sFLIM imaging data resulted in 16-fold increase in computation speed, which is a significant improvement over previous data analysis workflow<sup>27</sup>.

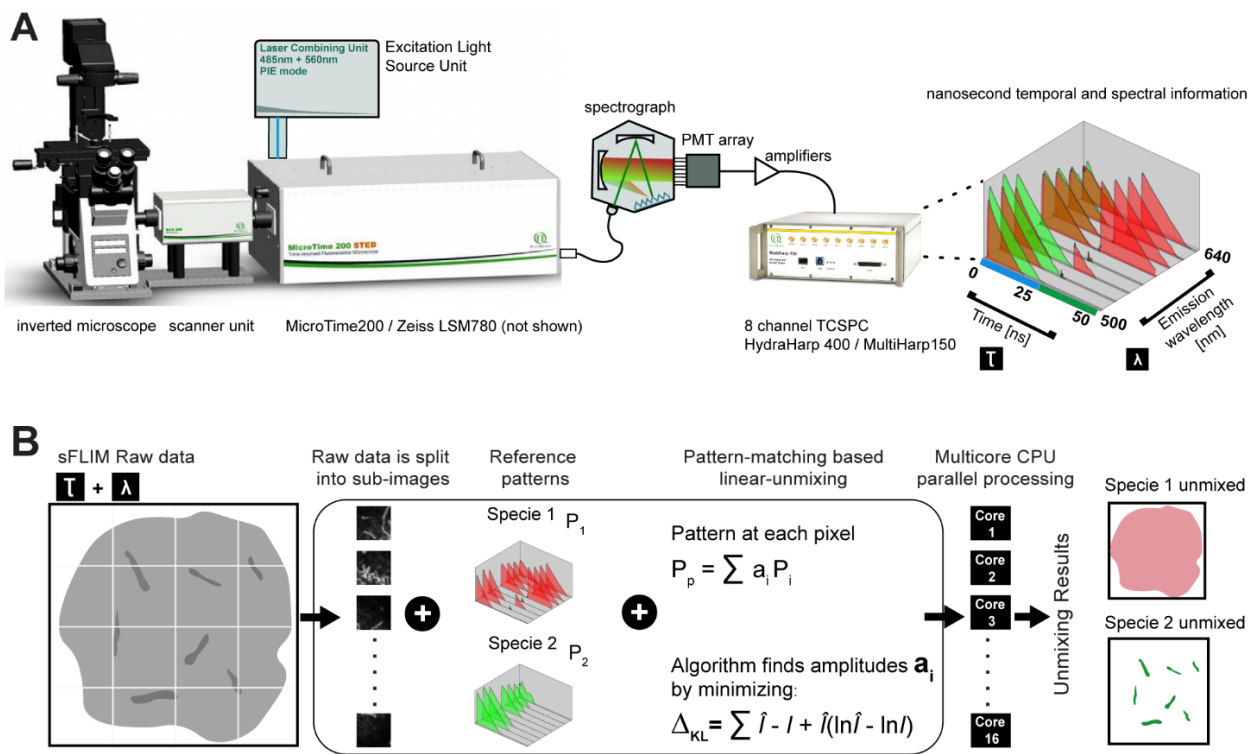


**Figure 2:** (A) Schematic illustration of the spectral-FLIM experimental setup developed for this research work. Sample excitation is performed using lasers with wavelength 485 nm and 561 nm operating in pulsed interleaved mode. The emitted fluorescence signal is detected with a combination of an 8-channel photomultiplier tube array connected to an 8-channel TCSPC unit (HydraHarp 400 or MultiHarp 150). For each detected photon in image pixel, information is recorded about its arrival time in addition to which spectral emission channel it belongs to. The complete detection systems allow for simultaneous recording of emitted multi-dimensional signals, combining spectral and nanosecond fluorescence decay properties of fluorescent labels. (B) We show the working principle of the pattern-matching algorithm of sFLIM datasets based on a linear-unmixing model. From left or right, acquired sFLIM datasets were first split into sub-images. Each of these sub-images along with a copy of reference patterns corresponding to species 1 and 2 are analyzed in parallel on a multi-core CPU using an open-source pattern-matching software custom written in MATLAB. The algorithm allows for clear separation of the fluorescence signal of co-localized species 1 and 2 into

independent channels in a precise manner. (A) is adapted and modified from Rohilla *et al.* 2020 (see *Supplementary Fig. 2-3*)<sup>24</sup>.

## **2.4 Fluorescence lifetime analysis**

The SymPhoTime software (PicoQuant, Germany) was used to obtain lifetime values by performing fitting of fluorescence decays with a bi-exponential decay model re-convolved with the measured instrument response function (IRF). To account for the distortions of fluorescence decays at higher count rates due to pulse pile-up effects, we used a bi-exponential rapid re-convolution fitting model to obtain correct lifetime values<sup>38</sup>. The quality of fit was judged on the reduced chi-square values and corresponding normally distributed fitting residuals after every iterative step. In this work, intensity as well as amplitude weighted average lifetime values were reported for each bi-exponential fit. The lifetime values are reported as mean  $\pm$  SD from at least three independent experiments.

## **2.5 Generation of reference patterns**

For the best results, the reference patterns were generated by imaging the single or FRET-pair stained cells and tissue samples using the described sFLIM setup. All the photons from selected regions of interest (ROIs) in a sFLIM image were merged to generate one multi-dimensional reference pattern corresponding to a labelled or AF structure. One such reference pattern includes information like excitation laser wavelength, spectral detection channel and shape of the nanosecond fluorescence decay. It is very important that all the sample preparation and imaging conditions (cell lines, AB incubation time, chemicals for washing, laser power, pixel dwell time, TCSPC base resolution etc.) are kept the same for all prepared samples.

## **2.6 Bleed-through calculation**

Throughout this report, bleed-through and cross-talk are used interchangeably. It is defined as the incorrect attribution of photons from one unmixed colour channel to another unmixed channel. The bleed-through calculations are performed using unmixed images obtained after pattern-matching-based unmixing analysis of raw sFLIM data. The bleed-through analysis was first proposed by Winter *et al.* (see “residual crosstalk calculation”, Materials and Methods)<sup>39</sup>, and we adapted this routine to compute

percentage bleed-through numbers. The analysis works best when regions of pixels are selected such that they only represent contribution from one species. Sometimes, one cellular structure will completely overlap other species, e.g. pan-cytokeratin is omnipresent in cells and overlaps mitochondria or the golgi apparatus in cells. In this case, it becomes difficult to perform bleed-through analysis. To carry out the bleed-through computation in this special scenario, we performed pattern-matching-based unmixing for single stained sample data using all the reference patterns employed during multi- stained sample unmixing (see 10. Paper I Results). This simple solution makes it possible to quantify bleed-through of overlapping species into different unmixed colour channels. For tissue AF samples, it was straightforward to compute bleed-through numbers as regions with pure species were much easier to find.

## **2.7 Statistical analysis**

GraphPad Prism 7 (version 7.01) was used throughout this project for statistical analysis. An unpaired two-tailed Student's *t*-test was used to compute the significant changes in donor fluorophore lifetime after the acceptor fluorophore mixing step, and the significance level ( $\alpha$ ) of 0.05 was considered significant (Fig. 5). The results are reported as mean  $\pm$  SD from at-least three independent experiments.

## **2.8 Data and code availability**

The pattern-matching software package used in this study is available for download at the link: [www.github.com/SumeetRohilla/sFLIM](https://www.github.com/SumeetRohilla/sFLIM). The data generated and used for this research work is included in published articles and this report.

### 3. RESULTS

#### 3.1. Paper I: Multi-target IMF by leveraging cross-labelling antibody artefacts and spectral-FLIM-FRET detection<sup>24</sup>.

**Cross-labelling between secondary antibodies leads to FRET.** First, it was reasoned that changes in the photophysical properties of fluorophores on interacting cross-labelled secondary ABs caused by FRET could be used to precisely separate the fluorescence signal of cross- and single-labelled species into different analysis colour channels<sup>25</sup>. As a preliminary step, secondary ABs “goat-anti-rabbit Alexa488” (donor) and “rabbit-anti-mouse Alexa555” (acceptor) were chosen as cross-labelling FRET AB pair. As non-cross-labelling zero FRET control, I chose secondary ABs “goat-anti-rabbit Alexa488” and “goat-anti-mouse Alexa555”. For fluorescence lifetime quantification, time-domain FLIM and SymPhoTime 64 analysis software were used. Next, measured fluorescence decays were fitted to obtain lifetime values of free secondary ABs in aqueous solution (Table 1). Finally, non- as well as cross-labelling secondary AB pairs were mixed together and were measured using time-domain FLIM to quantify changes in the donor fluorophore lifetimes due to possible FRET interactions. As hypothesized, we observed no change in donor fluorophore lifetime for the non-cross-labelling AB pair (Fig. 3A), whereas a significant decrease in donor fluorophore lifetime was observed exactly after the AB mixing step at time  $t = 60$  s (Fig. 3B). This characteristic change in donor fluorophore lifetime is a clear indication of FRET ( $\Delta\tau_{\text{int}} = 0.66$  ns, difference between unquenched and quenched donor lifetime) for the interacting fluorophores on the cross-labelling AB pair.

sAb-fluorophore conjugate	Type	antibody : H <sub>2</sub> O		Excitation $\lambda_{\text{exc}}$ [nm]	Emission $\lambda_{\text{ems}}$ [nm]	Lifetime $\tau_{\text{int}}$ [ns]	Std. dev. $\tau_{\text{int}}$ [ns]	Lifetime $\tau_{\text{amp}}$ [ns]	Std. dev. $\tau_{\text{amp}}$ [ns]
		[ $\mu\text{L}$ ]							
goat-anti-rabbit Alexa488	F(ab) <sub>2</sub> IgG (H+L)	5 : 500		485	500 - 555	3.84	0.03	3.68	0.02
goat-anti-mouse Alexa555	F(ab) IgG1 (lambda L)	5 : 500		561	574 - 650	0.93	0.04	0.73	0.04
rabbit-anti-mouse Alexa555	F(ab) <sub>2</sub> IgG (H+L)	5 : 500		561	574 - 650	0.89	0.03	0.71	0.03
rabbit-anti-mouse Alexa546	F(ab) <sub>2</sub> IgG (H+L)	5 : 500		561	574 - 650	3.58	0.06	3.31	0.05
goat-anti-rabbit Alexa546	F(ab) <sub>2</sub> IgG (H+L)	5 : 500		561	574 - 650	3.49	0.02	3.33	0.03

sAb, secondary antibody

**Table 1:** Fluorescence lifetime values of free fluorophore-tagged secondary antibodies (ABs) in aqueous solutions. Measurements were performed using the sFLIM system. Lifetime quantification was performed using SymPhoTime 64 software. Intensity ( $\tau_{\text{int}}$ ) as well amplitude ( $\tau_{\text{amp}}$ ) averaged lifetime values are reported here for each bi-exponential fit. Lifetime data is given as mean  $\pm$  SD from three independent experiments. Adapted and modified from Rohilla *et al.* 2020 (see *Supplementary Table*)<sup>24</sup>.

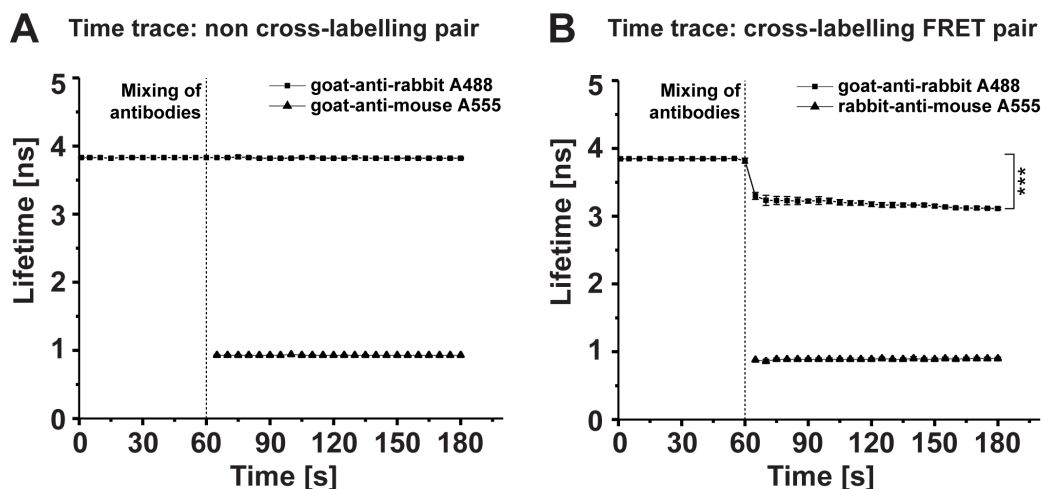


**Figure 3:** Results of fluorescence lifetime quantification for mixing of two pairs of fluorophore-tagged secondary ABs. **(A)** Non-cross-labelling secondary ABs (“goat-anti-rabbit Alexa488” and “goat-anti-mouse Alexa555”) do not exhibit any change in their lifetime values of  $3.83 \pm 0.10$  ns and  $0.93 \pm 0.10$  ns, respectively. **(B)** Use of cross-labelling FRET AB pair (“goat-anti-rabbit Alexa488” and “rabbit-anti-mouse Alexa555”) leads to FRET interactions between donor (Alexa488) and acceptor (Alexa555) fluorophores resulting in observed characteristic decrease of donor fluorophore lifetime from  $3.84 \pm 0.01$  ns to  $3.18 \pm 0.04$  ns ( $\Delta\tau_{\text{int}} = 0.66$  ns). Fluorescence lifetime values are given as mean  $\pm$  SD from three independent experiments; \*\*\* $p < 0.001$ . Adapted and modified from Rohilla *et al.* 2020 (see Fig. 3)<sup>24</sup>.

**Triple antigen IMF using just two fluorophores and sFLIM-FRET.** In this section, it is shown that by leveraging cross-labelling AB FRET effects and sFLIM detection system, it becomes possible to achieve triple antigen IMF of A549 cells for TOM20, pan-cytokeratin and golgin with a combination of two species for primary AB host species (rabbit, mouse) as well as two fluorophore-tagged secondary ABs (“rabbit-anti-mouse Alexa546” and “goat-anti-rabbit Alexa488”). By following a proposed labelling sequence, pan-cytokeratin was positive for “rabbit-anti-mouse Alexa546”, TOM20 for “goat-anti-rabbit Alexa488” and golgin for “rabbit-anti-mouse Alexa546” (Fig. 4). This labelling scheme led to an additional labelling of pan-cytokeratin with “goat-anti-rabbit Alexa488” as well as “rabbit-anti-mouse Alexa546” secondary ABs, and inevitably, resulting in FRET effects between interacting fluorophores on cross-labelled ABs.

First, as a prerequisite, FRET effects were verified on pan-cytokeratin due to cross-labelling of the “rabbit-anti-mouse Alexa546” and “goat-anti-rabbit Alexa488” AB pair. For quantification of FRET effects, a donor-only labelled pan-cytokeratin (no FRET) control sample was also prepared. The sFLIM measurements and subsequent fluorescence lifetime analysis (Table 2) of cross-labelled and donor-only labelled pan-cytokeratin sample shows clear signs of FRET effects ( $\Delta\tau_{\text{int}} = 0.67$  ns, difference



between unquenched and quenched donor lifetime) caused by interaction between fluorophores on cross-labelled ABs. Next, I demonstrate the inability of conventional filter-based imaging methods to separate the fluorescence signals of cross- and single labelled antigens into independent analysis channels (Fig. 5A). In addition, one could notice that there is significant false-positive attribution of the pan-cytokeratin signal in the TOM20 and golgin channel (Channel mode imaging, Fig. 5A). Finally, we showed that use of sFLIM imaging followed by pattern-matching-based data analysis enabled us to quantitatively separate the fluorescence contributions from all three immunolabelled antigens into their independent fluorescence analysis channels notwithstanding the complexity due to strong overlapping of TOM20 and golgin by the pan-cytokeratin structure (Fig. 5B)<sup>24</sup>. To achieve optical unmixing results, it is important to generate reference patterns for TOM20 and golgin from control samples, whereas the pan-cytokeratin reference sample was obtained from a triple antigen IMF sample (Fig. 5C).

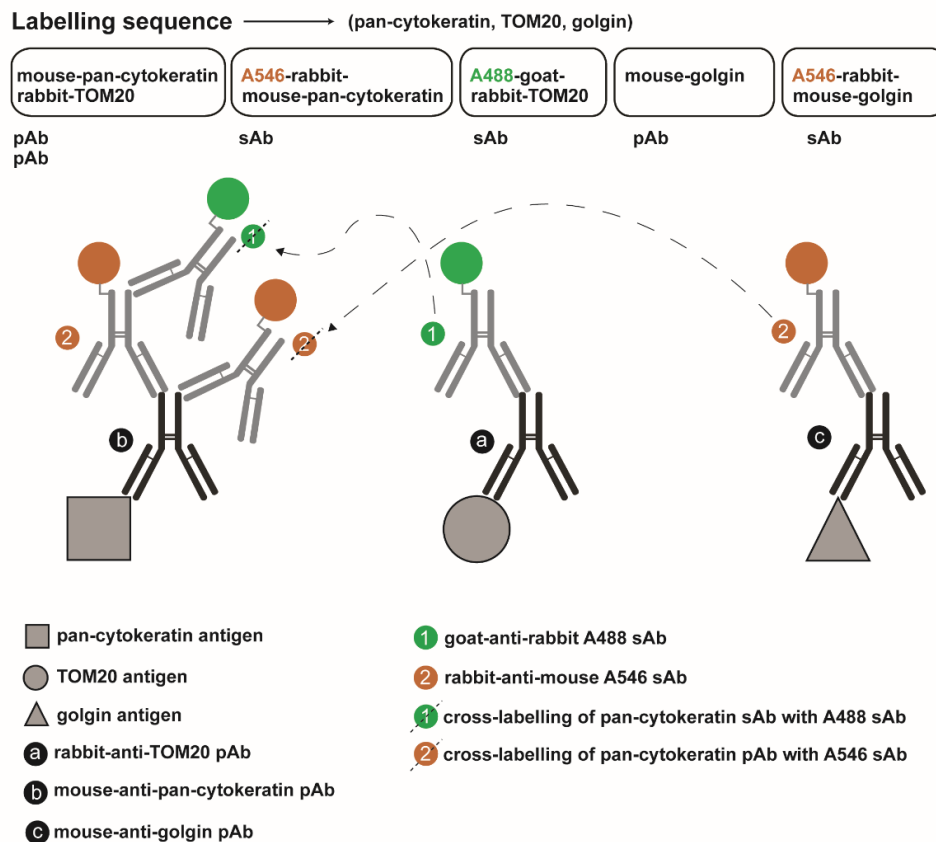


**Figure 4:** The illustration shows a labelling strategy for triple antigen immunofluorescence (IMF) on A549 cells using just two primary (rabbit, mouse) and corresponding fluorophore-tagged secondary antibody (AB) (“goat-anti-rabbit Alexa488” and “rabbit-anti-mouse Alexa546”) species types. Following sequential labelling steps, cells were labelled for pan-cytokeratin (“rabbit-anti-mouse Alexa546”), TOM20 (“goat-anti-rabbit Alexa488”) and golgin (“rabbit-anti-mouse Alexa546”). This labelling procedure led to cross-labelling of pan-cytokeratin with FRET fluorophore-AB pair

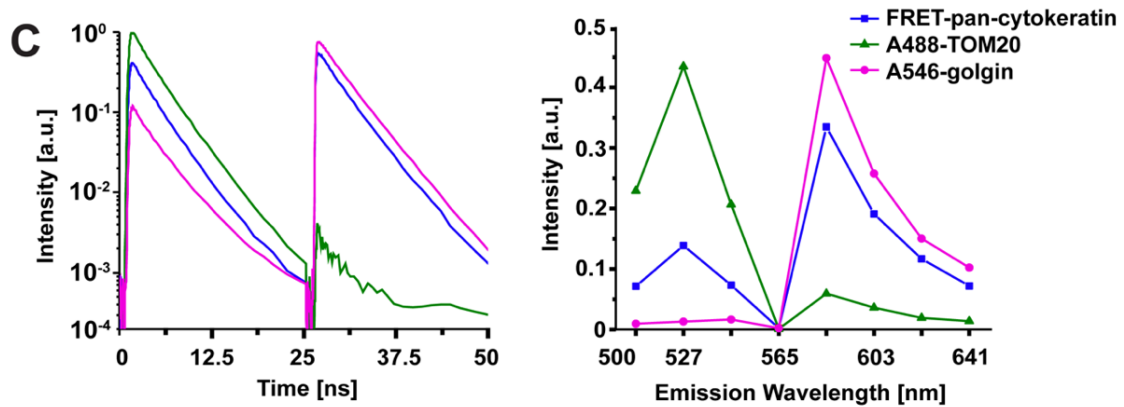
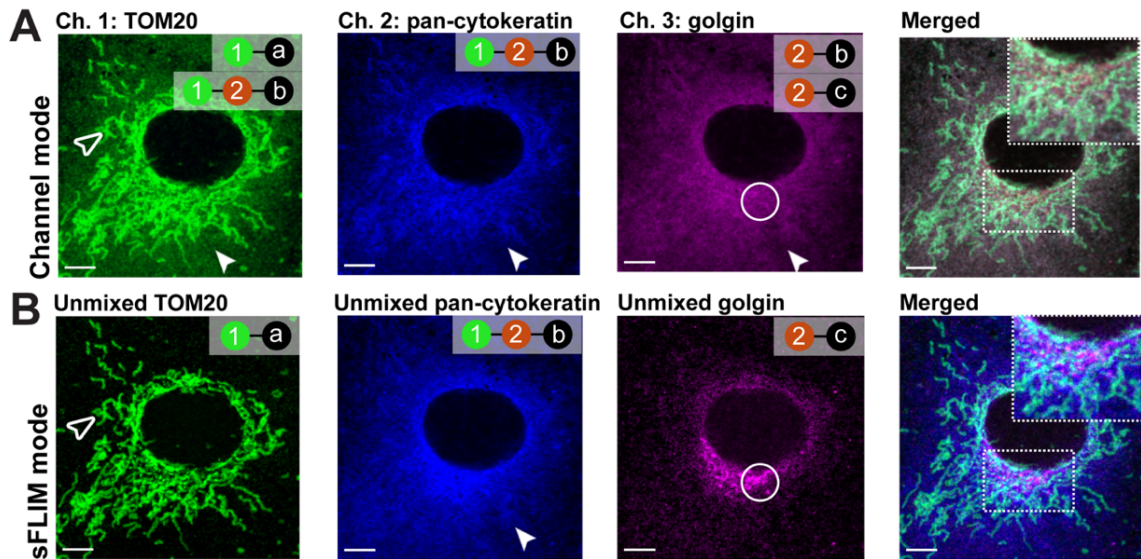
(Alexa488 and Alexa546). This cross-labelling of pan-cytokeratin and resulting FRET signature is assigned a new fluorescence channel and thus it becomes possible to quantitatively separate three antigens via use of spectral-FLIM-FRET. Adapted and modified from Rohilla *et al.* 2020 (see *Supplementary Fig. 4*)<sup>24</sup>.

Immunolabelling			Target	Excitation $\lambda_{exc}$ [nm]	Emission $\lambda_{ems}$ [nm]	Fluorophore	Lifetime $\tau_{int}$ [ns]	Std. dev. $\tau_{int}$ [ns]	Lifetime $\tau_{amp}$ [ns]	Std. dev. $\tau_{amp}$ [ns]
principal	cross ( <sup>1</sup> )	cross ( <sup>2</sup> )								
unconjugated rabbit-anti-mouse	goat-anti-rabbit A488	-	pan-cytokeratin	485	500 - 555	Alexa488	2.38	0.03	2.18	0.03
rabbit-anti-mouse A546	goat-anti-rabbit A488	rabbit-anti-mouse A546	pan-cytokeratin	485	500 - 555	Alexa488	1.71	0.04	1.15	0.05
goat-anti-rabbit A488	-	-	TOM20	485	500 - 555	Alexa488	2.28	0.06	2.07	0.04
rabbit-anti-mouse A546	-	-	golgin	561	574 - 650	Alexa546	2.84	0.09	2.53	0.03
rabbit-anti-mouse A546	-	-	pan-cytokeratin	561	574 - 650	Alexa546	2.79	0.05	2.54	0.03

(<sup>1</sup>) represents cross-labelling of pan-cytokeratin with Alexa488 after TOM20 principal labelling step

(<sup>2</sup>) represents cross-labelling of pan-cytokeratin with Alexa546 after golgin principal labelling step

**Table 2.** Excitation and emission maxima as well as fluorescence lifetimes were determined using the spectral-FLIM (sFLIM) system. Lifetime values obtained from sFLIM measurements of A549 cells immunolabelled for TOM20 (“goat-anti-rabbit Alexa488”) and golgin (“rabbit-anti-mouse Alexa546”) as well as pan-cytokeratin with cross-labelling ABs (“goat-anti-rabbit Alexa488” and “rabbit-anti-mouse Alexa546”) exhibiting FRET. In addition, a donor-only (“goat-anti-rabbit Alexa488” AB) labelled pan-cytokeratin sample was imaged to obtain the donor-only fluorophore lifetime value for FRET quantification on pan-cytokeratin. Intensity( $\tau_{int}$ )- and amplitude( $\tau_{amp}$ )-weighted fluorescence lifetime values are given as mean  $\pm$  SD from three independent experiments. Adapted and modified from Rohilla *et al.* 2020 (see *Supplementary Table*)<sup>24</sup>.



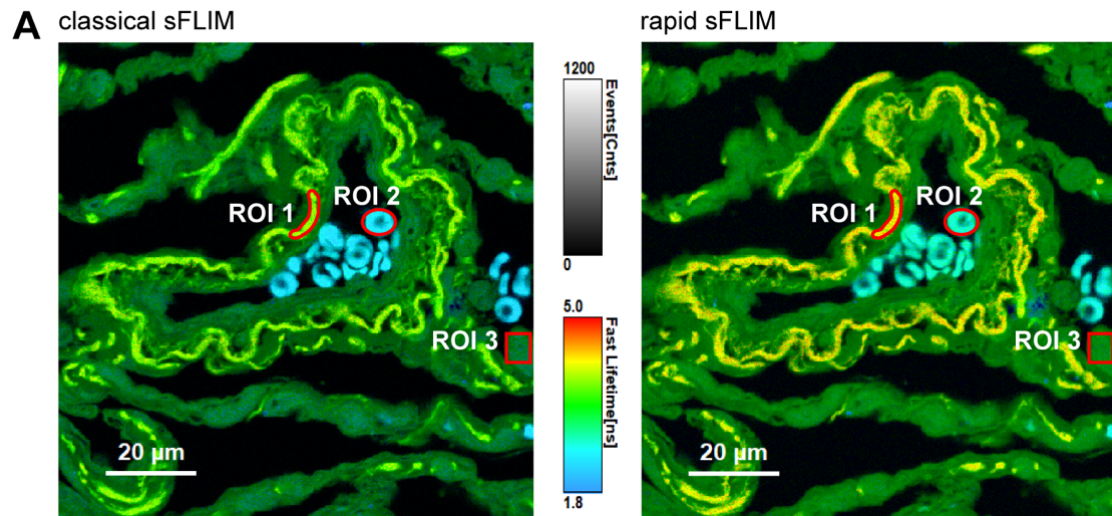
- a** rabbit-anti-TOM20 pAb
- b** mouse-anti-pan-cytokeratin pAb
- c** mouse-anti-golgin pAb
- 1** goat-anti-rabbit A488 sAb
- 2** rabbit-anti-mouse A546 sAb
- 1-2** cross-labelling of pan-cytokeratin with A488 and A546 sAb

**Figure 5:** A549 cells were labelled for three target antigens with just two primary (rabbit, mouse) and secondary antibody (AB) (“goat-anti-rabbit Alexa488”; “rabbit-anti-mouse Alexa546”) host species types. Following the labelling procedure as shown in Fig. 7, we achieved single labelling of TOM20 (with “goat-anti-rabbit Alexa488”) and golgin (with “rabbit-anti-mouse Alexa546”) as well as cross-labelling of pan-cytokeratin (with “rabbit-anti-mouse Alexa546” and “goat-anti-rabbit Alexa488”). **(A)** Conventional channel mode imaging was shown to be insufficient for eliminating attribution from pan-cytokeratin (closed arrowhead) in the TOM20 and golgin channel. **(B)** The spectra-FLIM data acquisition and pattern-matching analysis enables clear visualization of all three antigens into independent analysis channels with a notable false-positive suppression (see merged images in A and B panel). **(C)** Shown are the reference patterns, combining sub-nanosecond fluorescence decays (left panel, 485 nm and 561 nm excitation laser wavelengths were used) and emission spectra (right panel) information, used in the pattern-matching algorithm for unmixing of fluorescence contributions from singly labelled TOM20 (Alexa488) and golgin (Alexa546) as well as FRET AB pair labelled pan-cytokeratin. Representative images from three independent experiments are shown; scale bars 5  $\mu$ m. Adapted and modified from Rohilla *et al.* 2020 (see Fig. 5)<sup>24</sup>.

### **3.2. Paper II: Rapid-sFLIM enables faster time-resolved imaging of biological samples with very high data throughput<sup>36</sup>.**

Historically, in FLIM measurements of biological samples, the major bottleneck is the slow data acquisition rates due to longer dead times (or time duration in which the detection system is insensitive to a second photon after one photon was detected) of TCSPC electronics as well as the requirement of detecting no more than a photon-event per every 10 excitation laser pulses, collectively termed classical-sFLIM measurement mode in this study. Typical dead time for a detection unit (Photomultiplier tubes; PMT) is between 10 and 100 ns, while the dead time for TCSPC electronics is about 100 ns<sup>40</sup>. To address this limitation, PicoQuant developed a sub-nanosecond low dead time 8-channel TCSPC unit (MultiHarp150), and this new device was used to demonstrate the high-throughput capability with parallel data acquisition in synchronous but spectrally independent detection channels, defined as rapid-sFLIM measurement mode. Human lung tissue samples were measured using the sFLIM system equipped with a MultiHarp 150 TCSPC instrument (Fig. 2A). First, by limiting the data acquisition stop times to 1500 photons in the brightest pixel, we show the speedup gains provided by rapid-sFLIM mode over classical-sFLIM measurements (Fig. 6). The data analysis reveals that the rapid-sFLIM system (Fig. 6A, right panel) enables six times faster data acquisition compared with classical-sFLIM (Fig. 6A, left panel). Furthermore, a maximum count rate of 65 Mcps (summed over all detection channels) was reached in the brightest pixels compared to a meagre 11 Mcps under a classical-sFLIM measurement regime.

Next, we evaluated the lifetime values obtained under two operation regimes for three distinct AF species in human lung tissue – red blood cells (RBCs), collagen and alveolar macrophages (AM) (Fig. 6). A rapid-reconvolution bi-exponential fitting model was used for lifetime quantification and also included a correction parameter accounting for fluorescence decay distortions at high detection count rates (see Wahl *et al.* 2020, Fig. 7, 9)<sup>36</sup>. Compared to classical-sFLIM data analysis, a systematic lifetime increase of 0.1 ns was observed for all measured regions using rapid-sFLIM mode. This is primarily a limitation of the fitting model and ongoing work aims at resolving this systematic discrepancy in lifetime estimation by rapid-sFLIM measurements. Altogether, in this work it was shown that the rapid-sFLIM system allows for 7 times faster data acquisition compared to conventional multi-channel TCSPC FLIM measurements, with reliable estimation of fluorescence lifetime values.



**B**

ROI	Autofluorescent Species	Lifetime $\pm$ std. dev. [ns]	
		classical sFLIM	rapid sFLIM
1	Collagen	$3.6 \pm 0.02$	$3.7 \pm 0.01$
2	RBCs <sup>a</sup>	$2.4 \pm 0.01$	$2.5 \pm 0.01$
3	AM <sup>b</sup>	$2.7 \pm 0.01$	$2.8 \pm 0.02$

<sup>a</sup>RBCs: red blood cells  
<sup>b</sup>AM: alveolar macrophage

**Figure 6:** Unstained human lung tissue samples were measured using the rapid spectral-FLIM system. **(A)** Shown are mean photon arrival time images of highly autofluorescent human lung tissue samples measured under classical-sFLIM (left) and rapid-sFLIM (right) operational limits. **(B)** Fluorescence decays from selected regions of interest (ROIs) for collagen (ROI 1), red blood cells (RBCs; ROI 2) and alveolar macrophages (AM; ROI 3) were fitted to obtain lifetime value. Fluorescence lifetime values are given as mean  $\pm$  SD from three independent experiments; scale bars 20  $\mu$ m. Adapted and modified from Wahl *et al.* 2020 (see Fig. 8-9)<sup>36</sup>.

### **3.3. Outlook research: Simultaneous autofluorescence and multi-target immunofluorescence imaging in human lung tissue samples by sFLIM.**

#### **Characterization of AF species in human lung tissue samples by spectral-FLIM**

Fig. 6A shows different autofluorescent species in lung tissue samples, where contrast between different structures arises due to their distinct fluorescence lifetime properties. Based on these observations, we reasoned that FLIM provides better contrast compared to multi-spectral imaging (MSI) and this could be used as a potential tool for precise characterization of AF species in human lung tissue samples. In this view, we imaged three ROIs per each tissue sample obtained from 20 different patients using the rapid-sFLIM detection system. First, to select regions of pixels with similar lifetime properties, we used fast-FLIM image data (Fig. 7A, left panel) to generate a decay diversity map (Fig. 7A, right panel; a scatterplot of  $\tau_{avg}$  versus  $\sigma_{\tau}$ ). It is important to note that different AF structures have pronounced maxima or clusters (Fig 7A, right panel, marked in different colours) in decay diversity map which was consistent for all imaged lung tissue samples. In light of these observations, I decided to classify the lung tissue AF, broadly, into three distinct categories – erythrocytes (or RBCs), collagen and cytosolic (which includes AM compartments). In this way, we derived a total of 180 patterns - 3 (per each AF species) x 3 (per each ROI) x 20 patients from measured sFLIM datasets. Fig. 7B shows all 180 AF patterns and their corresponding fluorescence decay (left panel) obtained via two pulsed laser excitation (485 nm and 561 nm) and spectra emission curves. It can immediately be seen that patterns from different AF structures cluster together very nicely under 485 nm excitation (0 - 25ns pulse duration) and, based on these differences, can be easily separated from each other although they were derived from different patients (Fig. 7B, left panel). Also, there is no clear distinction between patterns from different AF species based on their emission spectra (Fig. 7B, right panel), meaning that addition of fluorescence lifetime decay information to the unmixing algorithm should potentially lead to improved separation of AF species into different analysis channels. To prove this, we performed unmixing analysis using spectral-only (Fig. 7C) and total sFLIM information (Fig. 7D). Furthermore, corresponding percentage bleed-through numbers were calculated and are shown in Table 4. A direct comparison of unmixed erythrocytes and cytosolic AF (Fig. 7C and 7D) clearly shows that, compared to spectral-only unmixing, generating unmixed images using sFLIM information results in less signal bleed-through. This was quantified and demonstrated using bleed-through



analysis (Table 3A and 3B). Together, this suggests that recoding of fluorescence lifetime decay in combination with emission spectra will result in much improved discrimination of endogenous fluorophores with minimal channel cross-talk.

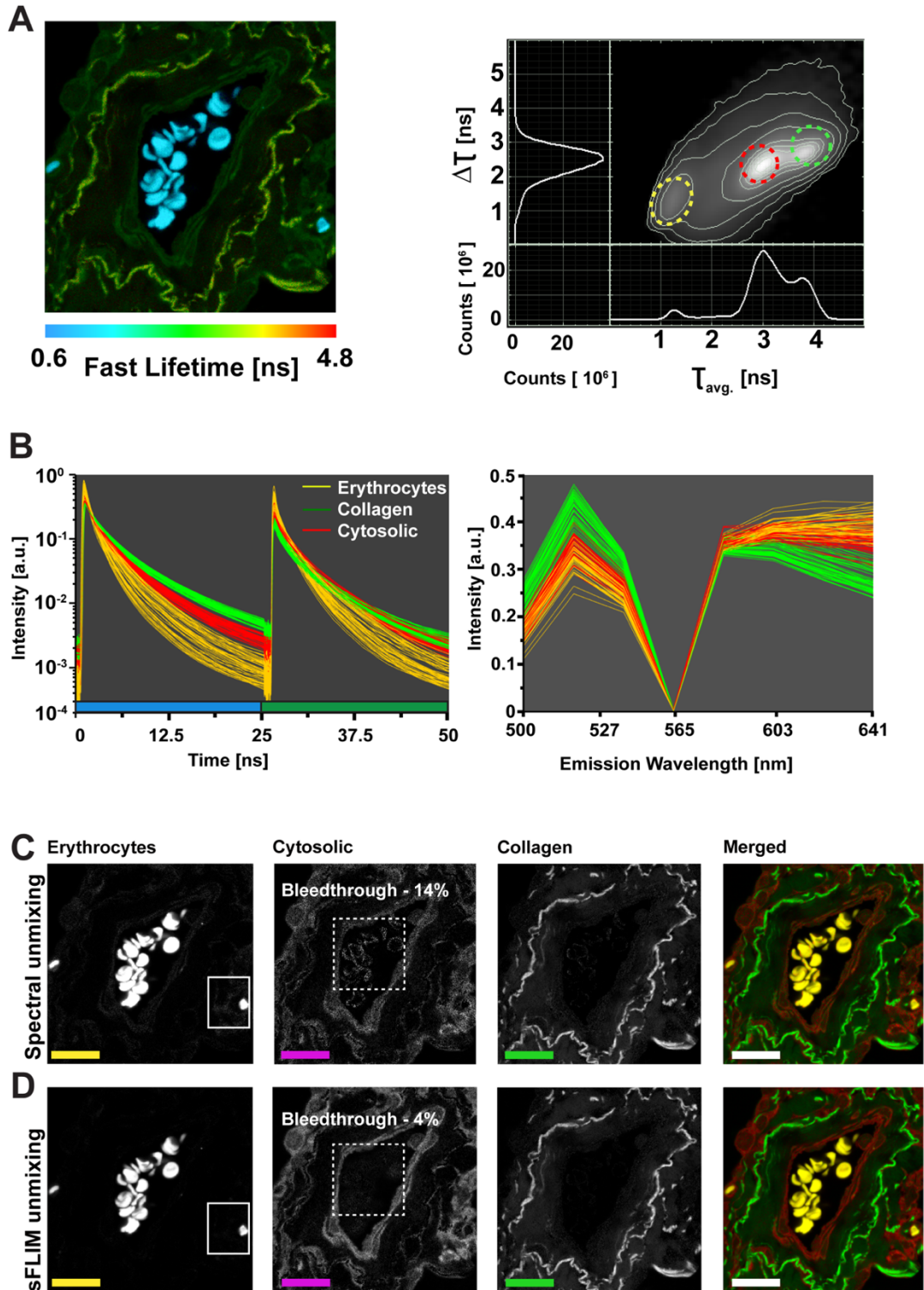


**Figure 7:** Shown above is a systematic method for identification and separation of different autofluorescent species in histological sections of human lung tissue. Tissue samples from 20 patients were imaged and analyzed using sFLIM and pattern-matching techniques. (A) Representative mean photon arrival time image (left panel) and corresponding

decay diversity map. This map is utilized to select groups of pixels with similar lifetime properties corresponding to a particular AF structure (erythrocytes - yellow; collagen - green and cytosolic - red). **(B)** A total of 180 patterns (20 patients X 3 AF species X 3 ROIs) were derived using this process and plotted along fluorescence decay (left panel; corresponding to two pulsed laser excitations, 485 nm marked as a blue bar and 561 nm marked as a green bar) and spectral dimension (right panel; dip at 565 nm due to notch filter for 561 nm excitation laser). **(C)** and **(D)** Representative unmixed images obtained by pattern-matching-based unmixing using spectral-only and total sFLIM information. We observe less channel bleed-through for sFLIM between unmixed channel images (dashed boxes) compared to spectral-only unmixing results. For percentage bleed-through numbers, see Table 3; scale bars 20  $\mu\text{m}$ .

<b>A</b>	<b>Channel bleedthrough [%]</b>	Cytosolic	Collagen	Erythrocytes
	Cytosolic	100	3.31	14.58
	Collagen	4.67	100	2.14
	Erythrocytes	12.35	10.59	100

<b>B</b>	<b>Channel bleedthrough [%]</b>	Cytosolic	Collagen	Erythrocytes
	Cytosolic	100	3.94	6.41
	Collagen	1.23	100	0.92
	Erythrocytes	1.92	0	100

**Table 3:** Quantitative bleed-through between unmixed images/channels after pattern-matching analysis of autofluorescent human lung tissue sample using **(A)** spectral and **(B)** total sFLIM (combining lifetime and spectral) information in reference patterns. The table must be read line-wise. The bleed-through reading of the first line (cytosolic) is therefore: 14.58% of unmixed cytosolic signal bleeding into the unmixed erythrocytes channel; see Materials and Methods for details). A significant reduction in signal bleed-through for all species is observed for sFLIM unmixing analysis mode compared to spectral-only analysis.

**Leveraging cross-labelling AB FRET effects and sFLIM for triple protein IMF in human lung tissue using just two fluorophores.** Next, we adapted our previously proposed FRET AB-pair cross-labelling method<sup>24</sup> to perform triple labelling of the following structures in highly autofluorescent lung tissues: EMP, proSPC and CD68. Following a sequential labelling procedure, single labelling of EMP (with “goat-anti-rabbit Alexa546”), proSPC (with “goat-anti-rabbit Alexa488”) and CD68 (with “goat-anti-mouse Alexa546”) was achieved. This resulted in cross-labelling of EMP with FRET AB pair (Alexa488 and Alexa546). The sFLIM measurements and subsequent fluorescence lifetime analysis of cross-labelled and donor-only labelled EMP samples shows clear signs of FRET effects ( $\Delta\tau_{\text{int}} = 0.56$  ns, difference between unquenched and quenched donor lifetime) caused by interaction between fluorophores on cross-labelled ABs. Finally, multiplexed samples were imaged using sFLIM system. The resulting merged and unmixed single-target images clearly show that sFLIM detection and pattern-matching analysis enables clear separation of fluorescence contributions from single (proSPC and CD68) and cross-labelled (EMP) structures as well as three AF species



into an independent colour analysis channel in a robust manner with minimal bleed-through by using sFLIM detection and pattern-matching algorithm (Fig. 8A). Reference patterns used in pattern-matching analysis are shown in Fig. 8B. For optimal results, we prepared single labelled control samples to derive reference patterns for proSPC and CD68, whereas a pure AF-only sample from the same patient was used to obtain AF reference patterns.

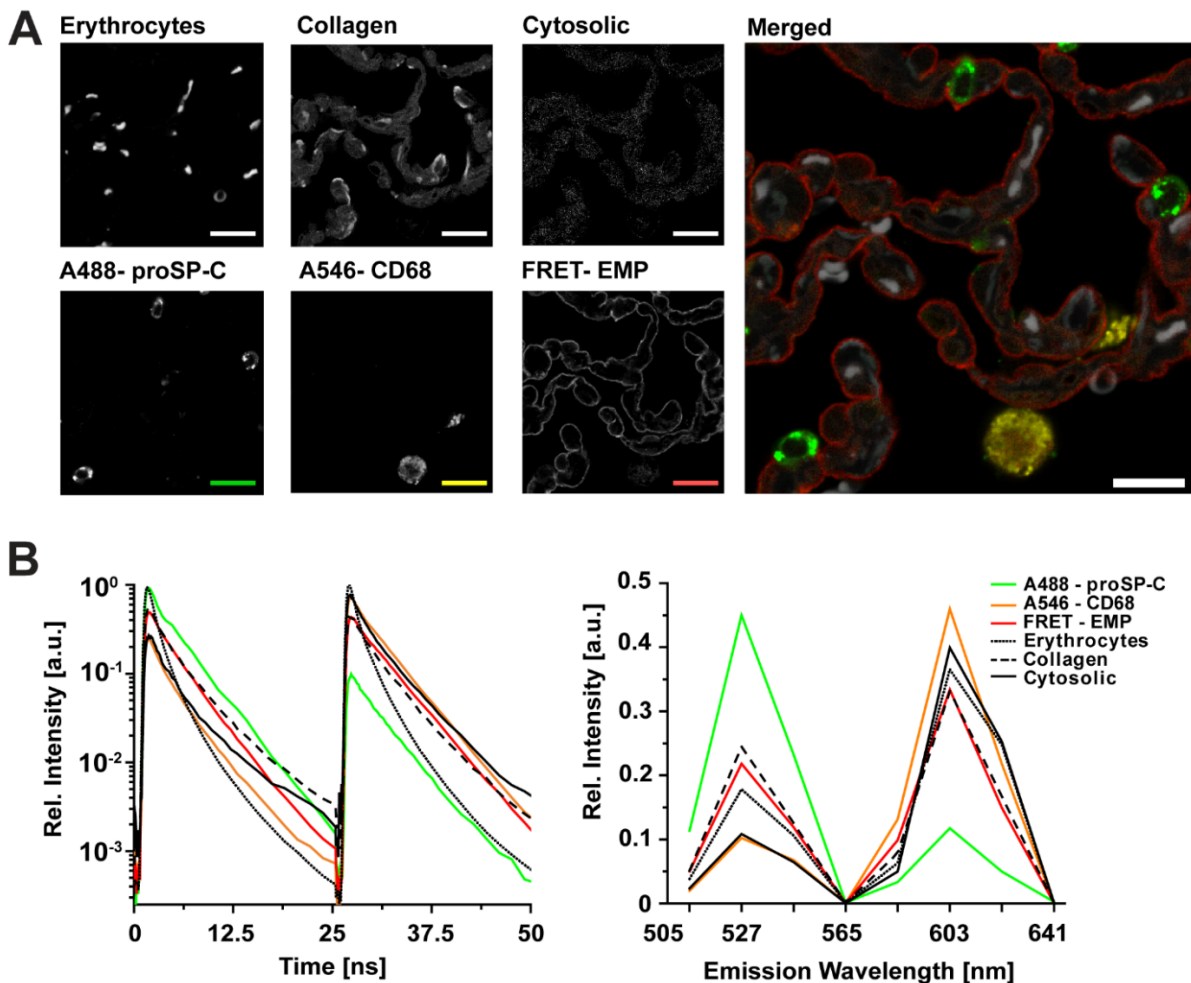


**Figure 8:** Human lung tissue samples were immunolabelled for three different target proteins (extracellular matrix protein, EMP; pro-surfactant protein, proSPC; phagocytic cluster of protein 68, CD68) with just two primary (rabbit, mouse) and fluorophore-tagged secondary antibody (“goat-anti-rabbit-Alexa546”, “goat-anti-rabbit-Alexa488” and “goat-anti-mouse Alexa546”) species types. Following a sequential labelling procedure, single labelling of proSPC (with Alexa488) and CD68 (with Alexa546) as well as cross-labelling of EMP (with Alexa488 and Alexa546) was achieved. The multiplexed tissue sample was imaged and analyzed using sFLIM and a pattern-matching algorithm, respectively. **(A)** Shown are the resulting merged and single target images of EMP (red), proSPC (green), CD68 (yellow) and three lung tissue autofluorescent (AF in white) species (erythrocytes, collagen and cytosolic), clearly visualized in three independent channels. **(B)** The six (3 x protein targets, 3 x AF species) corresponding reference patterns: fluorescence decays (left panel) corresponding to two alternating laser pulses and emission spectra (right panel) with gap introduced due to notch filter to avoid direct detection of scattered 561 nm laser light; scale bars 15  $\mu\text{m}$ .

## 4. DISCUSSION AND CONCLUSION

---

In this research work, a novel immunolabelling strategy was proposed to overcome the limitations posed by false-positive cross-labelling in cellular as well as tissue IMF scenarios. A sequential immunolabelling procedure was described that includes appropriate selection of fluorophore tagged secondary ABs serving as suitable FRET pairs. Next, sFLIM imaging and pattern-matching-based analysis was performed to attribute these FRET signals from cross-labelled structures to independent fluorescence analysis channels. To demonstrate the potential of the method, triple antigen IMF in cells as well as in highly autofluorescent lung tissue was carried out using just two fluorophores, which would be impossible to separate by conventional filter-based imaging in cross-labelling conditions. Furthermore, the newly developed eight-channel rapid-sFLIM system was shown to overcome classical pile-up limitation through a low dead-time TCSPC device, enabling high data throughput (up to 65 Mcps) for fast FLIM measurements of fixed tissue samples. Finally, the study of label-free lung tissue samples from 20 different patients using sFLIM imaging and pattern-matching analysis elucidates that combining fluorescence lifetime information with spectral emission properties provides better contrast and reduced channel bleed-through compared to multi-spectral imaging for discrimination of inherent autofluorescent species. Based on these results, the combined approach of sFLIM detection and pattern-matching analysis proves that the wealth of information (spectral as well fluorescence lifetime decay) recorded by this system allows for clear separation of differently labelled targets in multiplexed IMF scenarios with minimal channel bleed-through, even in the presence of strong background AF.

A key advantage of the proposed IMF scheme is that it requires only the design of suitable AB labelling sequences and subsequent controls for achieving efficient FRET effects on double labelled antigens. In other words, well-performing IMF protocols with established primary ABs can be maintained in laboratories, thereby avoiding the time and cost expense of establishing new IMF kits for false-positive cross-labelling. Although previous studies have shown that it is possible to visualize two antigens simultaneously using primary ABs raised in same species<sup>11,14,15</sup>, these methods additionally require an intermediate blocking step with AB F(ab) fragments for the first staining. This results in higher background signals, i.e. poor SNR due to non-specific binding of blocking AB

fragments, and consequently, decreased intensity of first labelling, possibly due to over-blocking of AB on the first antigen<sup>11</sup>. Franzusoff *et al.* proposed a similar method that required the primary ABs to be pre-saturated in chemical solution to avoid any cross-labelling from same species fragments, but also reported that this could possibly reduce the affinity of the primary ABs to target antigens<sup>17</sup>. More recently, Tsurui *et al.* reported a method for seven-colour analysis of IMF stained tissue using monoclonal ABs treated with avidin biotin complex (ABC)<sup>13</sup>. The use of high ABC ratios allows for increased SNR and specificity, but also bears the risk of increased unspecific background signal from avidin bound to endogenous biotin in cells as well as tissues. Furthermore, these studies use channel-mode imaging for sequential excitation and subsequent filter-based detection of each fluorophore colour, and data analysis requires additional dummy exposure images to correct for signal bleed-through from shorter wavelength dye groups into the red one. In comparison, our AB multiplexing method expands the fluorophore tagging options using already available ABs from the same host species. In addition, sFLIM detection systems enable simultaneous excitation due to PIE and acquisition of spectral as well as temporal profiles via multi-channel TCSPC detection. More importantly, the pattern-matching algorithm combines decay and spectral information to provide better unmixing with improved SNR and minimal bleed-through, thereby enabling precise fluorophore channel attribution post unmixing analysis.

Time-domain FLIM is highly preferred, and is often considered to be the gold standard for quantitative FRET in the scientific community, but it is technically demanding, as demonstrated in the study by Pelet *et al.*<sup>34</sup>. Similar methods such as acceptor photobleaching or sensitized emission are intensity-based methods which could also be used for FRET analysis, but would be totally insufficient to identify and recover signals in scenarios where both single- as well cross-labelled species are present in one sample. In recent work of Arsenovic *et al.*, it was demonstrated that sensitized emission in spectral unmixing mode is possible but still requires careful calibration procedures, and is limited only to specific combinations of donor and acceptor excitation laser<sup>41</sup>. Furthermore, since their method only uses emission spectra of fluorophores, any presence of background AF with an overlapping spectral profile will add uncertainty to the unmixing process and reduce the accuracy of FRET measurement. Compared to these limitations of an MSI system, a spectral-FLIM detection system with PIE excitation involves the flexibility to choose any donor-acceptor pair, and provides improved FRET

quantitation analysis. Furthermore, the benefits of unmixing based on the combination of FLIM with spectral domain has been demonstrated in recent work, where it was shown that separation quality decreased substantially when spectral or only lifetime information was used separately for unmixing<sup>27</sup>. In AF as well as multi-target tissue sample studies, similar results were observed and it was demonstrated that sFLIM will provide better unmixing results in more complex scenarios where fluorophore emission spectra are strongly overlapping. In total, the ability of the sFLIM detection and pattern-matching analysis to unambiguously separate fluorophores with spectroscopically similar fluorescence signatures or even cross-labelling FRET ABs, as shown throughout this study, will probably expand the fluorophore multiplexing toolbox, enabling multiple targets to be imaged and visualized simultaneously.

While one may take advantage of our proposed labelling procedure leveraging FRET effects between cross-labelling ABs, obstacles and limitations that hinder the direct adaptation into routine experiments are still present. For example, some ABs are simply FRET incompatible due to their large molecule size or one might be tempted to use higher AB concentrations for achieving higher FRET effects<sup>24</sup>. Hence, as a first step it is a necessary prerequisite to perform control studies to ensure FRET interactions between fluorophore-tagged ABs, first in solution, then in cells, and if required, in tissue staining also. Researchers must determine, through trial and error, the optimal primary and secondary AB concentrations to avoid artefacts due to unspecific or background staining. Furthermore, the choice of labelling sequence is of critical importance to achieve FRET labelling on target antigens. For example, in triple cellular IMF, performing the TOM20 labelling first will result in cross-labelling of pan-cytokeratin with “rabbit-anti-mouse Alexa546” AB, which makes it difficult to separate from golgin due to their similar spectral and fluorescence decay properties. Another key aspect of this labelling procedure is the use of F(ab) fragments for cross-labelling ABs as opposed to full IgG molecules. As was shown by Holzapfel *et al.*, former AB fragment types will exhibit stronger and observable FRET on cross-labelling antigens compared to full IgG molecules. This is due to the fact that full IgG molecules are large compared to F(ab) fragments and allow for reduced possibility of interaction between donor and acceptor fluorophores.

The development of a rapid-sFLIM system is another major improvement over the previous system used in the work of Niehörster *et al.*<sup>27</sup>. The new multi-dimensional

sFLIM detection system has high detection efficiency due to the inclusion of highly sensitive multi-array PMTs with GaAsP cathodes and faster speed of acquisition due to independent as well as parallelized multi-channel TCSPC units with ultra-low dead times. With this parallelized detection approach and new fast timing electronics hardware, we showed that lifetime measurements are not limited by the classical pile-up limit, which enables a significant boost in data acquisition (higher frame rate) at high detection count rates, simultaneously covering a broad spectral range<sup>24,36</sup>.

In conclusion, a novel AB-based multiplexing approach is presented that allows researchers to use the adversity arising from cross-labelling artefacts in IMF to their advantage and, at the same time, provides a general solution for multiplex IMF using AB originating in the same host species. I hope that this possibility will allow researchers to develop individual labelling schemes based on already well-established primary ABs combined with the use of several commercially available fluorophore-tagged secondary ABs that are FRET compatible pairs (e.g. Cy3 / Cy5 or ATTO488 / ATTO565 etc.). With this work, I envisage that (rapid)-sFLIM and pattern-matching analysis has the potential to serve as an innovative imaging method that will benefit the entire research field in which AB-based IMF is carried out and will potentially enable differentiation between cancerous and normal tissue based on their AF properties alone. I believe that sFLIM imaging will yield excellent multicolour imaging results and facilitate new discoveries in biomedical as well as clinical research.

## 5. BIBLIOGRAPHY

---

- 1 Lichtman, J. W. & Conchello, J. A. Fluorescence microscopy. *Nature methods* **2**, 910-919, doi:10.1038/nmeth817 (2005).
- 2 Eliyatkin, N., Yalçın, E., Zengel, B., Aktaş, S. & Vardar, E. Molecular Classification of Breast Carcinoma: From Traditional, Old-Fashioned Way to A New Age, and A New Way. *J Breast Health* **11**, 59-66, doi:10.5152/tjbh.2015.1669 (2015).
- 3 Tan, D. & Zander, D. S. Immunohistochemistry for assessment of pulmonary and pleural neoplasms: a review and update. *Int J Clin Exp Pathol* **1**, 19-31 (2008).
- 4 Feng, Z., Jensen, S. M., Messenheimer, D. J., Farhad, M., Neuberger, M., Bifulco, C. B, Fox, B. A., Multispectral Imaging of T and B Cells in Murine Spleen and Tumor. *The Journal of Immunology* **196**, 3943, doi:10.4049/jimmunol.1502635 (2016).
- 5 Stack, E. C., Wang, C., Roman, K. A. & Hoyt, C. C. Multiplexed immunohistochemistry, imaging, and quantitation: A review, with an assessment of Tyramide signal amplification, multispectral imaging and multiplex analysis. *Methods* **70**, 46-58, doi:10.1016/j.ymeth.2014.08.016 (2014).
- 6 Coons, A. H., Leduc, E. H. & Connolly, J. M. Studies on antibody production. I. A method for the histochemical demonstration of specific antibody and its application to a study of the hyperimmune rabbit. *The Journal of Experimental Medicine* **102**, 49-60, doi:10.1084/jem.102.1.49 (1955).
- 7 Mohan, K., Pai, S., Rao, R., Sripathi, H. & Prabhu, S. Techniques of immunofluorescence and their significance. *Indian Journal of Dermatology, Venereology, and Leprology* **74**, 415-419, doi:10.4103/0378-6323.42898 (2008).
- 8 Warford, A., Howat, W. & McCafferty, J. Expression profiling by high-throughput immunohistochemistry. *Journal of immunological methods* **290**, 81-92, doi:10.1016/j.jim.2004.04.010 (2004).
- 9 Fritschy, J. M. Is my antibody-staining specific? How to deal with pitfalls of immunohistochemistry. *The European journal of neuroscience* **28**, 2365-2370, doi:10.1111/j.1460-9568.2008.06552.x (2008).
- 10 Ramos-Vara, J. A. Technical aspects of immunohistochemistry. *Veterinary pathology* **42**, 405-426, doi:10.1354/vp.42-4-405 (2005).
- 11 Lewis, C. S. A., Gillete-Ferguson, I. & Ferguson, D. G. An indirect immunofluorescence procedure for staining the same cryosection with two mouse monoclonal primary antibodies. *Journal of Histochemistry & Cytochemistry* **41**, 1273-1278, doi:10.1177/41.8.7687266 (1993).
- 12 Negoescu, A., Labat-Moleur, F., Lorimier, P., Lamarcq, L., Guillermet, C., Chambaz, E., Brambilla, E., F(ab) secondary antibodies: a general method for double immunolabelling with primary antisera from the same species. Efficiency control by chemiluminescence. *Journal of Histochemistry & Cytochemistry* **42**, 433-437, doi:10.1177/42.3.7508473 (1994).
- 13 Tsurui, H., Nishimura, H., Hattori, S., Hirose, S., Okumura, K., Shirai, T., Seven-color fluorescence imaging of tissue samples based on Fourier spectroscopy and singular value decomposition. *Journal of Histochemistry & Cytochemistry* **48**, 653-662, doi:10.1177/002215540004800509 (2000).

- 14 Valnes, K. & Brandtzaeg, P. Comparison of paired immunofluorescence and paired immunoenzyme staining methods based on primary antisera from the same species. *Journal of Histochemistry & Cytochemistry* **30**, 518-524, doi:10.1177/30.6.6178779 (1982).
- 15 Wurden, S. & Homberg, U. A simple method for immunofluorescent double staining with primary antisera from the same species. *Journal of Histochemistry & Cytochemistry* **41**, 627-630, doi:10.1177/41.4.8450202 (1993).
- 16 Pirici, D., Mogoanta, L., Kumar-Singh, S., Pirici, I., Margaritescu, C., Simionescu, C., Stanescu R., Antibody Elution Method for Multiple Immunohistochemistry on Primary Antibodies Raised in the Same Species and of the Same Subtype. *Journal of Histochemistry & Cytochemistry* **57**, 567-575, doi:10.1369/jhc.2009.953240 (2009).
- 17 Franzusoff, A., Redding, K., Crosby, J., Fuller, R. S. & Schekman, R. Localization of components involved in protein transport and processing through the yeast Golgi apparatus. *The Journal of Cell Biology* **112**, 27-37, doi:10.1083/jcb.112.1.27 (1991).
- 18 Yaziji, H. & Barry, T. Diagnostic Immunohistochemistry: what can go wrong? *Advances in anatomic pathology* **13**, 238-246, doi:10.1097/01.pap.0000213041.39070.2f (2006).
- 19 Bendayan, M. Possibilities of false immunocytochemical results generated by the use of monoclonal antibodies: the example of the anti-proinsulin antibody. *Journal of Histochemistry & Cytochemistry* **43**, 881-886, doi:10.1177/43.9.7642961 (1995).
- 20 Mighell, A. J., Hume, W. J. & Robinson, P. A. An overview of the complexities and subtleties of immunohistochemistry. *Oral diseases* **4**, 217-223 (1998).
- 21 Peter, A., Fatykhova, D., Kershaw, O., Gruber, A. D., Rueckert, J., Neudecker, J., Toennies, M., Bauer, T. T., Schneider, P., Schimek, M., Eggeling, S., Suttorp, N., Hocke, A. C., Hippenstiel, S., Localization and pneumococcal alteration of junction proteins in the human alveolar-capillary compartment. *Histochemistry and cell biology* **147**, 707-719, doi:10.1007/s00418-017-1551-y (2017).
- 22 Mansfield, J. R., Gossage, K. W., Hoyt, C. C. & M.D., R. M. L. Autofluorescence removal, multiplexing, and automated analysis methods for in-vivo fluorescence imaging. *Journal of biomedical optics* **10**, 1-9, 9 (2005).
- 23 Wang, M., Long, F., Tang, F., Jing, Y., Wang, X., Yao, L., Ma, J., Fei, Y., Chen, L., Wang, G., Mi, L., Autofluorescence Imaging and Spectroscopy of Human Lung Cancer. *Applied Sciences* **7**, 32 (2017).
- 24 Rohilla, S., Krämer, B., Koberling, F., Gregor, I. & Hocke, A. C. Multi-target immunofluorescence by separation of antibody cross-labelling via spectral-FLIM-FRET. *Scientific Reports* **10**, 3820, doi:10.1038/s41598-020-60877-8 (2020).
- 25 Holzapfel, H. Y. & Birtwistle, M. R. Creating complex fluorophore spectra on antibodies through combinatorial labeling. *Translational science* **2** (2016).
- 26 Lakowicz, J. R. *Principles of Fluorescence Spectroscopy*. (Springer US, 2013).
- 27 Niehörster, T., Löscherger, A., Gregor, I., Krämer, B., Rahn, H. J., Patting, M., Koberling, F., Enderlein, J., Sauer, M., Multi-target spectrally resolved fluorescence lifetime imaging microscopy. *Nature methods* **13**, 257-262, doi:10.1038/nmeth.3740 (2016).
- 28 Strat, D., Dolp, F., Einem, B., Steinmetz, C., Arnim, C. A., Rueck, A., Spectrally resolved fluorescence lifetime imaging microscopy: Forster resonant energy transfer

- global analysis with a one- and two-exponential donor model. *Journal of biomedical optics* **16**, 026002, doi:10.1117/1.3533318 (2011).
- 29 Popleteeva, M., Haas, K. T., Stoppa, D., Pancheri, L., Gasparini, L., Kaminski, C. F., Cassidy, L. D., Venkitaraman, A. R., Esposito, A., Fast and simple spectral FLIM for biochemical and medical imaging. *Optics express* **23**, 23511-23525, doi:10.1364/oe.23.023511 (2015).
- 30 Mansfield, J. R. Multispectral imaging: a review of its technical aspects and applications in anatomic pathology. *Veterinary pathology* **51**, 185-210, doi:10.1177/0300985813506918 (2014).
- 31 Zimmermann, T., Rietdorf, J. & Pepperkok, R. Spectral imaging and its applications in live cell microscopy. *FEBS Letters* **546**, 87-92, doi:10.1016/s0014-5793(03)00521-0 (2003).
- 32 Elangovan, M., Day, R. N. & Periasamy, A. Nanosecond fluorescence resonance energy transfer-fluorescence lifetime imaging microscopy to localize the protein interactions in a single living cell. *Journal of microscopy* **205**, 3-14 (2002).
- 33 Gratton, E., Breusegem, S., Sutin, J., Ruan, Q. & Barry, N. Fluorescence lifetime imaging for the two-photon microscope: time-domain and frequency-domain methods. *Journal of biomedical optics* **8**, 381-390, doi:10.1117/1.1586704 (2003).
- 34 Pelet, S., Previte, M. J. & So, P. T. Comparing the quantification of Forster resonance energy transfer measurement accuracies based on intensity, spectral, and lifetime imaging. *Journal of biomedical optics* **11**, 34017, doi:10.1117/1.2203664 (2006).
- 35 Chorvat, D. & Chorvatova, A. Multi-wavelength fluorescence lifetime spectroscopy: a new approach to the study of endogenous fluorescence in living cells and tissues. *Laser Physics Letters* **6**, 175-193, doi:10.1002/lapl.200810132 (2009).
- 36 Wahl, M., Röhlicke, T., Kulisch, S., Rohilla, S., Kraemer, B., & Hocke, C. A. Photon arrival time tagging with many channels, sub-nanosecond deadtime, very high throughput, and fiber optic remote synchronization. *Review of Scientific Instruments* **91**, 013108, doi:10.1063/1.5121412 (2020).
- 37 Wahl, M., Rahn, H. J., Röhlicke, T., Kell, G., Nettels, D., Hillger, F., Schuler, B., Erdmann, R., Scalable time-correlated photon counting system with multiple independent input channels. *Review of Scientific Instruments* **79**, 123113, doi:10.1063/1.3055912 (2008).
- 38 Patting, M., Reisch, P., Sackrow, M., Dowler, R., Koenig, M., Wahl, M., Fluorescence decay data analysis correcting for detector pulse pile-up at very high count rates. *Optical Engineering* **57**, 1-5, 5 (2018).
- 39 Winter, F., Loidolt, M., Westphal, V., Butkevich, A. N., Gregor, C., Sahl, S., and Hell, S. W., Multicolour nanoscopy of fixed and living cells with a single STED beam and hyperspectral detection. *Scientific Reports* **7**, 46492, doi:10.1038/srep46492 (2017).
- 40 Trinh, A. L., Ber, S., Howitt, A., Valls, P. O., Fries, M. W., Venkitaraman, A. R., Esposito, A., Fast single-cell biochemistry: theory, open source microscopy and applications. *Methods and Applications in Fluorescence* **7**, 044001, doi:10.1088/2050-6120/ab3bd2 (2019).
- 41 Arsenovic, P. T., Mayer, C. R. & Conway, D. E. SensorFRET: A Standardless Approach to Measuring Pixel-based Spectral Bleed-through and FRET Efficiency using Spectral Imaging. *Sci Rep* **7**, 15609, doi:10.1038/s41598-017-15411-8 (2017).



## 6. Contributions by Author

---

Sumeet Rohilla contributed the following to the below listed publication:

**Publication:** Sumeet Rohilla, Benedikt Krämer, Felix Koberling, Ingo Gregor, Andreas C. Hocke, Multi-target immunofluorescence by separation of antibody cross-labelling via spectral-FLIM-FRET. Sci Rep **10**, 3820, doi:10.1038/s41598-020-60877-8 (2020).

### Contribution:

<b>Conceptualization</b>	Designed the study by supervision of A. C. Hocke and B. Krämer
<b>Experiments</b>	<ul style="list-style-type: none"><li>• Immunolabelling strategy was developed and established under supervision of A. C. Hocke and B. Krämer (Fig. 1.)</li><li>• Samples were prepared by A. C. Hocke lab (Materials and Methods)</li><li>• Carried out optical setup and characterization of sFLIM system (Suppl. Fig. 2)</li><li>• Performed microscopy by supervision of B. Krämer and A. C. Hocke (Fig. 2 – 5)</li></ul>
<b>Analysis and software</b>	Developed software and analyzed data under the supervision of B. Krämer, I. Gregor and A. C. Hocke (Fig. 2 – 5, Suppl. Fig. 1 - 5)
<b>Manuscript</b>	Drafted the main text and prepared all figures
<b>Review and Editing</b>	All authors reviewed and edited the manuscript

---

Signature, date and stamp of first supervising university professor / lecturer

---

Signature of doctoral candidate

## 7. Statutory Declaration

---

“I, Sumeet Rohilla, by personally signing this document in lieu of an oath, hereby affirm that I prepared the submitted dissertation on the topic: “Novel biomedical applications for spectrally resolved fluorescence lifetime imaging microscopy”, independently and without the support of third parties, and that I used no other sources and aids than those stated.

All parts which are based on the publications or presentations of other authors, either in letter or in spirit, are specified as such in accordance with the citing guidelines. The sections on methodology (in particular regarding practical work, laboratory regulations, statistical processing) and results (in particular regarding figures, charts and tables) are exclusively my responsibility.

Furthermore, I declare that I have correctly marked all of the data, the analyses, and the conclusions generated from data obtained in collaboration with other persons, and that I have correctly marked my own contribution and the contributions of other persons (cf. declaration of contribution). I have correctly marked all texts or parts of texts that were generated in collaboration with other persons.

My contributions to any publications to this dissertation correspond to those stated in the below joint declaration made together with the supervisor. All publications created within the scope of the dissertation comply with the guidelines of the ICMJE (International Committee of Medical Journal Editors; [www.icmje.org](http://www.icmje.org)) on authorship. In addition, I declare that I shall comply with the regulations of Charité – Universitätsmedizin Berlin on ensuring good scientific practice.

I declare that I have not yet submitted this dissertation in identical or similar form to another Faculty.

The significance of this statutory declaration and the consequences of a false statutory declaration under criminal law (Sections 156, 161 of the German Criminal Code) are known to me.”

Date:

Signature

## Extract from the Journal summary list

Journal Data Filtered By: **Selected JCR Year: 2018** Selected Editions: SCIE,SSCI  
 Selected Categories: **"MULTIDISCIPLINARY SCIENCES"** Selected Category  
 Scheme: WoS

**Gesamtanzahl: 69 Journale**

Rank	Full Journal Title	Total Cites	Journal Impact Factor	Eigenfactor Score
1	NATURE	745,692	43.070	1.285010
2	SCIENCE	680,994	41.037	1.070190
3	National Science Review	1,842	13.222	0.006500
4	Science Advances	21,901	12.804	0.110010
5	Nature Communications	243,793	11.878	1.103290
6	Nature Human Behaviour	1,230	10.575	0.006550
7	PROCEEDINGS OF THE NATIONAL ACADEMY OF SCIENCES OF THE UNITED STATES OF AMERICA	661,118	9.580	1.022190
8	Science Bulletin	3,569	6.277	0.009840
9	Scientific Data	3,240	5.929	0.015610
10	Frontiers in Bioengineering and Biotechnology	1,994	5.122	0.006540
11	Journal of Advanced Research	2,691	5.045	0.004780
12	Research Synthesis Methods	1,932	5.043	0.005420
13	GigaScience	2,674	4.688	0.012510
14	Annals of the New York Academy of Sciences	46,385	4.295	0.025840
15	Scientific Reports	302,086	4.011	1.061540
16	Journal of the Royal Society Interface	12,933	3.224	0.029190
17	NPJ Microgravity	203	3.111	0.000670
18	PHILOSOPHICAL TRANSACTIONS OF THE ROYAL SOCIETY A- MATHEMATICAL PHYSICAL AND ENGINEERING SCIENCES	19,227	3.093	0.028200

OPEN

## Multi-target immunofluorescence by separation of antibody cross-labelling via spectral-FLIM-FRET

Sumeet Rohilla<sup>1,4</sup>, Benedikt Krämer<sup>2</sup>, Felix Koberling<sup>2</sup>, Ingo Gregor<sup>3</sup> & Andreas C. Hocke<sup>4\*</sup>

In biomedical research, indirect immunofluorescence labelling by use of primary and secondary antibodies is central for revealing the spatial distribution of multiple cellular antigens. However, labelling is regularly restricted to few antigens since species variation of primary and corresponding secondary antibodies is limited bearing the risk of unspecific cross-labelling. Here, we introduce a novel microscopic procedure for leveraging undesirable cross-labelling effects among secondary antibodies thereby increasing the number of fluorophore channels. Under cross-labelling conditions, commonly used fluorophores change chemical-physical properties by 'Förster resonance energy transfer' leading to defined changes in spectral emission and lifetime decay. By use of spectral fluorescence lifetime imaging and pattern-matching, we demonstrate precise separation of cross-labelled cellular antigens where conventional imaging completely fails. Consequently, this undesired effect serves for an innovative imaging procedure to separate critical antigens where antibody species variation is limited and allows for multi-target labelling by attribution of new fluorophore cross-labelling channels.

The technique of indirect immunofluorescence (IMF) by labelling antigens with primary and secondary antibodies (ABs) is still one of the most extensively used methods in microscopy to reveal the spatial distribution of molecules of interest in cells or tissues, thereby excellently serving to reach a deeper understanding of biological processes<sup>1</sup>. Next to careful planning of fixation, labelling sequences and proper AB controls, a further crucial aspect of IMF is the need for a stringent selection of primary and secondary AB pairs to avoid false-positive immunolabelling due to species overlap, especially if multiple antigens are targeted<sup>2,3</sup>. At best, primary ABs should originate from different species and combined with corresponding secondary ABs, all raised in one disparate host animal species or, at least, differing from the species origin of all primary and other secondary ABs (Fig. 1). Although a broad species panel of primary ABs is principally available (e.g. mouse, human, rabbit, rat, goat, chicken, sheep, guinea pig, hamster, bovine, donkey, dog, camelid, cat, pig etc.), practically, most specific and well-performing primary ABs for important target bio-molecules originate from mouse, rabbit, rat, or goat. Thus, if typical multi-target approaches include the repetitive labelling of organelles or structural proteins with established primary ABs, the combination of further molecules of interest is increasingly restricted by AB species overlap. A series of studies demonstrated how to overcome such problems for double immunolabelling using ABs produced in same species<sup>4-9</sup>. However, all these will finally still not completely avoid false-positive cross-labelling of desired antigens, bearing the risk of misinterpretation regarding (co-)localization, spatial distribution, or even interaction of molecules<sup>10-13</sup>.

But, what if such false-positive cross-labelling can be used as an advantage by generating new, independent fluorescence analysis channels? Indeed, this would transform cross-labelling due to species overlap of secondary ABs into a useful tool to expand IMF towards reliable and unambiguous multi-target labelling. A prerequisite to achieve this advantage is that single- as well as cross-labelled structures exhibit significant differences in their fluorescence characteristics allowing for precise separation and channel attribution. Like almost any dual fluorophore labelled bio-molecule with considerable overlap between their emission and absorption spectra, interacting fluorophores on ABs might change their chemical-physical properties by the so called 'Förster resonance energy transfer' (FRET), which was already nicely shown by previous work of Holzapfel *et al.*<sup>14</sup>. FRET occurs

<sup>1</sup>PicoQuant Innovations GmbH, Rudower Chaussee 29 (IGZ), 12489, Berlin, Germany. <sup>2</sup>PicoQuant GmbH, Rudower Chaussee 29 (IGZ), 12489, Berlin, Germany. <sup>3</sup>Third Institute of Physics, Georg-August-University, Friedrich-Hund-Platz 1, 37077, Göttingen, Germany. <sup>4</sup>Charité – Universitätsmedizin Berlin, corporate member of Freie Universität Berlin, Humboldt-Universität zu Berlin, and Berlin Institute of Health, Department of Internal Medicine/Infectious Diseases and Respiratory Medicine, Charitéplatz 1, 10117, Berlin, Germany. \*email: [andreas.hocke@charite.de](mailto:andreas.hocke@charite.de)

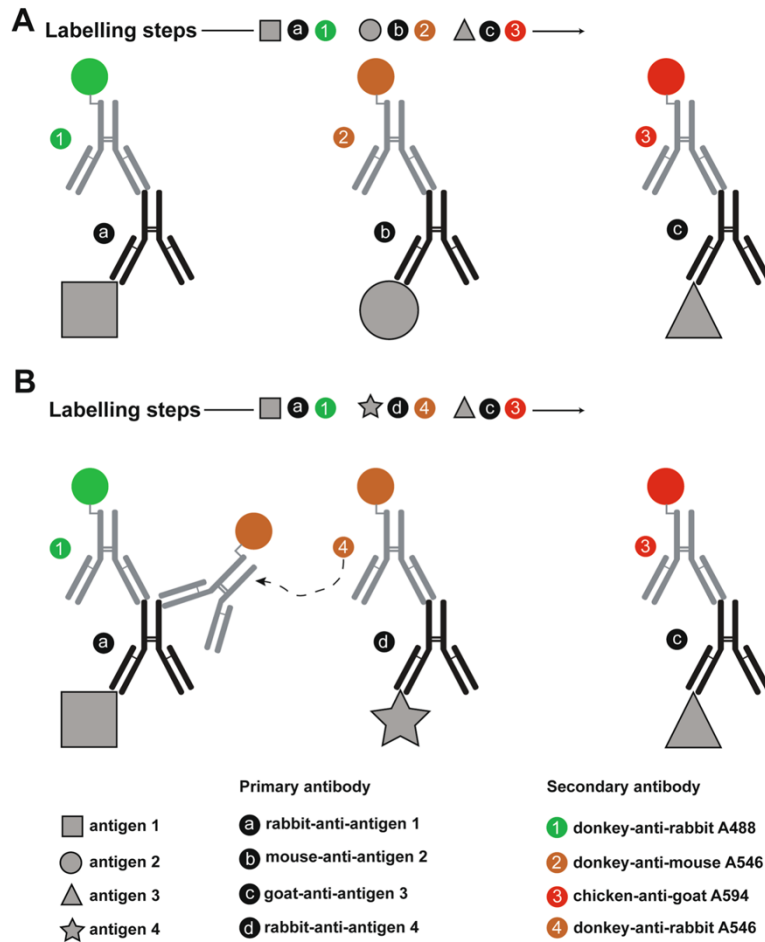


**Figure 1.** Non-cross- and cross-labelling in indirect immunofluorescence by secondary antibodies. Shown is a typical sequential labelling procedure used for indirect immunofluorescence (IMF) of three target antigens to demonstrate the resulting labelling in two scenarios. (A) Regular state: three different primary antibodies (ABs) origin from rabbit, mouse and goat bind to antigens 1, 2 and 3, respectively. For IMF detection, fluorophore-tagged secondary ABs (“donkey-anti-rabbit Alexa488”, “donkey-anti-mouse Alexa546” and “chicken-anti-goat Alexa594”), which are in origin different from that of targeted primary AB, will not show any cross-labelling. (B) Undesirable cross-labelling: primary ABs for antigens 1, 3 and 4 are originated from rabbit and goat. In this scenario, conjugation of secondary AB for IMF will lead to cross-labelling of rabbit primary AB for antigen 1 with “donkey-anti-rabbit Alexa546” leading to false-positive attribution of “donkey-anti-rabbit Alexa546” AB on antigen 1, bearing the risk of misinterpretation of results such as (co-)localization, spatial distribution, or even molecule-molecule interaction. For easy illustration purposes, a stoichiometry of 1:1 between primary and secondary AB is shown here, however in general, there are on an average more than one fluorophore attached to secondary AB. Similarly, depending on the available binding sites, the number of secondary AB bound to primary AB could vary between 2 to 5.

when fluorophores on cross-labelled ABs reach a physical proximity <10 nm resulting in a shift of two important characteristics, the fluorescence lifetime decay as well as the spectral emission. Therefore, by a combinatorial approach of measuring fluorescence lifetime decay as well as spectral information, cross-labelled structures could be precisely identified and separated from single labelled molecules. In a similar approach, we already demonstrated in the study of Niehörster *et al.* that the combinatorial use of fluorescence lifetime decay as well as spectral information is suitable for separation of up to nine different fluorophores in a cellular environment<sup>15</sup>. Here, we adapt this method to demonstrate that the use of cross-labelling due to species overlap enables us to introduce

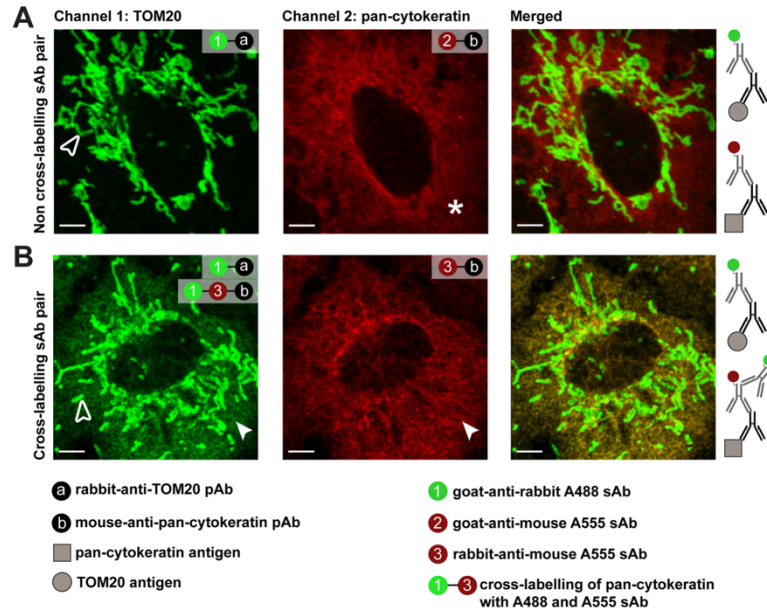


**Figure 2.** Channel mode imaging fails to separate cross-labelling in indirect immunofluorescence. (A) A549 cells were used to label two antigens, TOM20 and pan-cytokeratin, with a pair of non-cross-labelling secondary antibody (AB) (“goat-anti-rabbit Alexa488”, open arrowhead; “goat-anti-mouse Alexa555”, asterisk) resulting in correct-labelling and separation by channel mode imaging. (B) In contrast, labelling of TOM20 and pan-cytokeratin with a pair of cross-labelling AB species (“goat-anti-rabbit Alexa488”, open arrowhead; “rabbit-anti-mouse Alexa555”, closed arrowhead) resulted in false-positive attribution of pan-cytokeratin in TOM20 channel indicated by green cytosolic signal (closed arrowhead). Conventional channel mode imaging is demonstrated here as insufficient for eliminating channel cross-talk by cross-labelling of secondary ABs, even by using proper emission bandpass filters (520/14 nm and 593/20 nm). Representative images from three independent experiments are shown; scale bars 5  $\mu$ m.

new specific fluorescence analysis channels. To proof this hypothesis, we adapted a sequential IMF labelling protocol on A549 cells and selected appropriate fluorophore pairs on interacting secondary ABs to achieve FRET effects on cross-labelled cellular target molecules. Additionally, simultaneous acquisition and further processing of fluorescence lifetime decays as well as emission spectra necessitate proper hardware configuration and is again accomplished by means of time-domain spectrally resolved fluorescence lifetime imaging microscopy (sFLIM)<sup>15</sup>. As we and others already demonstrated, sFLIM combines the advantage of two non-filter based and independent confocal imaging modalities<sup>15–17</sup>. Multi-channel spectral imaging and time-resolved FLIM are combined for quantification of FRET interactions with high precision and single molecule sensitivity to detect and separate multiple distinct fluorescence channels<sup>18–22</sup>. Thus, we have built an 8-channel sFLIM detection system for quantification and verification of FRET signatures resulting from interaction of fluorophore labels on secondary ABs, which should demonstrate the capability to distinguish cross- and single-labelled target molecules in a typical biological IMF scenario. For data analysis we used an already established pattern-matching algorithm based on linear-unmixing which takes into account emission spectra as well as nanosecond fluorescence decays<sup>15</sup>.

In this proof-of-concept study, we could demonstrate how multiplexing in standard IMF gets possible with cross-labelled secondary ABs by the combination of multi-dimensional sFLIM and pattern-matching based unmixing achieving a minimum of bleed-through/cross-talk of fluorescence signals among different unmixed fluorescence analysis channels.

## Results

**Conventional channel mode imaging is insufficient to separate cross-labelled secondary antibodies.** In standard IMF, primary and secondary ABs are used to label different cellular antigens. By use of non-cross-labelling secondary ABs, conventional channel mode imaging shows a clear separation of fluorescence analysis channels if emission bandpass filters are properly configured. We first demonstrate A549 cells labelled for mitochondrial TOM20 and the structural protein pan-cytokeratin without any cross-labelling between secondary ABs (Fig. 2A). For this setting, channel mode imaging, either in wide-field or confocal mode, is fully sufficient to separate and allocate the two cellular antigens precisely. However, in case of species overlap leading to cross-labelling of one secondary AB with another, which is demonstrated here by “goat-anti-rabbit Alexa488” labelling of



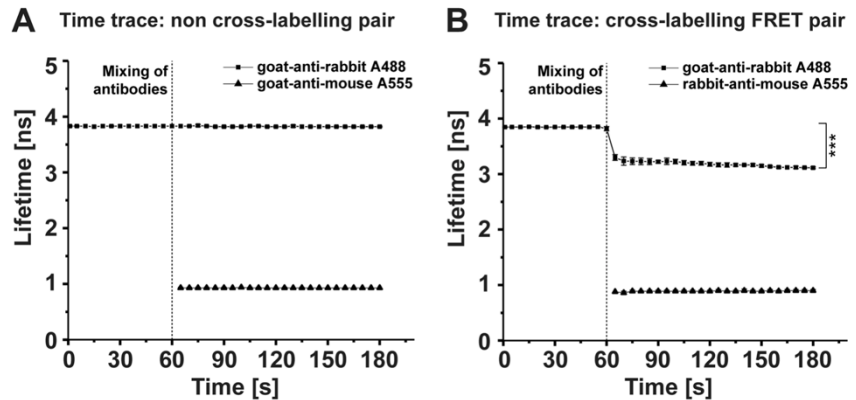


**Figure 3.** Cross-labelling of secondary antibodies leads to FRET. Two pairs of fluorophore-conjugated secondary antibodies (ABs) were mixed and measured for lifetime changes. (A) Non-cross-labelling ABs (“goat-anti-rabbit Alexa488” and “goat-anti-mouse Alexa555”) do not show any change of their average fluorescence lifetimes of about  $3.83 \pm 0.10$  ns and  $0.93 \pm 0.10$  ns, respectively. (B) Using cross-labelling secondary ABs (“goat-anti-rabbit Alexa488” and “rabbit-anti-mouse Alexa555”) leading to FRET, a significant shift of the donor fluorescence lifetime (Alexa488) from  $3.84 \pm 0.01$  ns to  $3.18 \pm 0.04$  ns ( $\Delta\tau_{int} = 0.66$  ns, intensity weighted lifetime) was measured. Quantification of donor and acceptor fluorescence lifetime is given as mean  $\pm$  SD from three independent experiments; \*\*\* $p < 0.001$ .

TOM20 *and* the secondary AB “rabbit-anti-mouse Alexa555”, a false-positive signal for pan-cytokeratin appears in the TOM20 channel indicating cytosolic co-localization of both antigens (Fig. 2B and see Supplementary Fig. 1 for labelling protocol). If such choices of secondary ABs cannot be avoided, even the proper setting of emission band pass filters is insufficient for signal separation showing the obvious limitation of conventional filter-based microscopic methods.

**Cross-labelling between secondary antibodies leads to FRET.** Since conventional channel mode imaging is insufficient to separate fluorophore emission of cross-labelled secondary ABs, we reasoned that the alteration of the photophysical properties of the used fluorophores caused by FRET will be suitable to address this issue<sup>44</sup>. As FRET pairs, we again chose the ABs “goat-anti-rabbit Alexa488” (donor) and “rabbit-anti-mouse Alexa555” (acceptor) as well as “goat-anti-rabbit Alexa488” and “goat-anti-mouse Alexa555” as non-cross-labelling negative control. Respective fluorescence lifetimes were quantified by standard time-correlated single-photon counting based fluorescence lifetime imaging microscopy (TCSPC-FLIM) and using the SymPhoTime 64 (PicoQuant, Germany) analysis software. As a first step, we obtained fluorescence lifetimes of free secondary ABs in aqueous solution (Supplementary Table 1A). Afterwards, non- as well as cross-labelling AB pairs were mixed, the AB concentrations were measured by fluorescence correlation spectroscopy (FCS) and, fluorescence lifetimes were quantified by TCSPC-FLIM in aqueous solution (Fig. 3). As hypothesised, no change in donor fluorophore lifetime was revealed for the non-cross-labelling AB pair (Fig. 3A), but a significant decrease in the donor fluorophore lifetime was observed directly after AB mixing at time  $t = 60$  s, clearly indicating FRET ( $\Delta\tau_{int} = 0.66$  ns, difference between unquenched and quenched donor fluorophore intensity weighted lifetime) for the cross-labelling AB pair (Fig. 3B). This analysis demonstrates that fluorophores conjugated to cross-labelling secondary ABs undergo FRET interaction, which might be suitable for separation in a cellular IMF scenario.

**Separation and new channel attribution for cross-labelled antibodies by sFLIM-FRET.** As demonstrated, cross-labelling secondary ABs undergo FRET interaction, which we now aimed to use as advantage in IMF for creating new fluorescence analysis channels by sFLIM. To demonstrate the potential of sFLIM for resolving undesired cross-labelling, we again performed dual antigen IMF as introduced in Fig. 2B. As a first step, we performed multi-dimensional fluorescence imaging of dual antigen IMF sample by sFLIM system (Supplementary Fig. 2, see Materials and Methods for system details). Using this system, we verified whether cross-labelling of pan-cytokeratin with secondary AB pairs resulted in FRET effects or not. A donor-only sample where pan-cytokeratin was cross-labelled with “goat-anti-rabbit Alexa488” and “unconjugated rabbit-anti-mouse” AB was used as control for FRET quantification on pan-cytokeratin. Fluorescence decays obtained by sFLIM measurements of FRET AB pair and donor-only labelled control samples were fitted to obtain quenched and unquenched donor lifetime using the SymPhoTime 64 software (Supplementary Table 1B). As hypothesized, we revealed that close binding of cross-labelling AB pairs on pan-cytokeratin indeed resulted in FRET ( $\Delta\tau_{int} = 0.47$  ns, difference between unquenched and quenched donor fluorophore intensity weighted lifetime). Next, as a prerequisite for sFLIM based quantitative separation, we first demonstrate again that separation

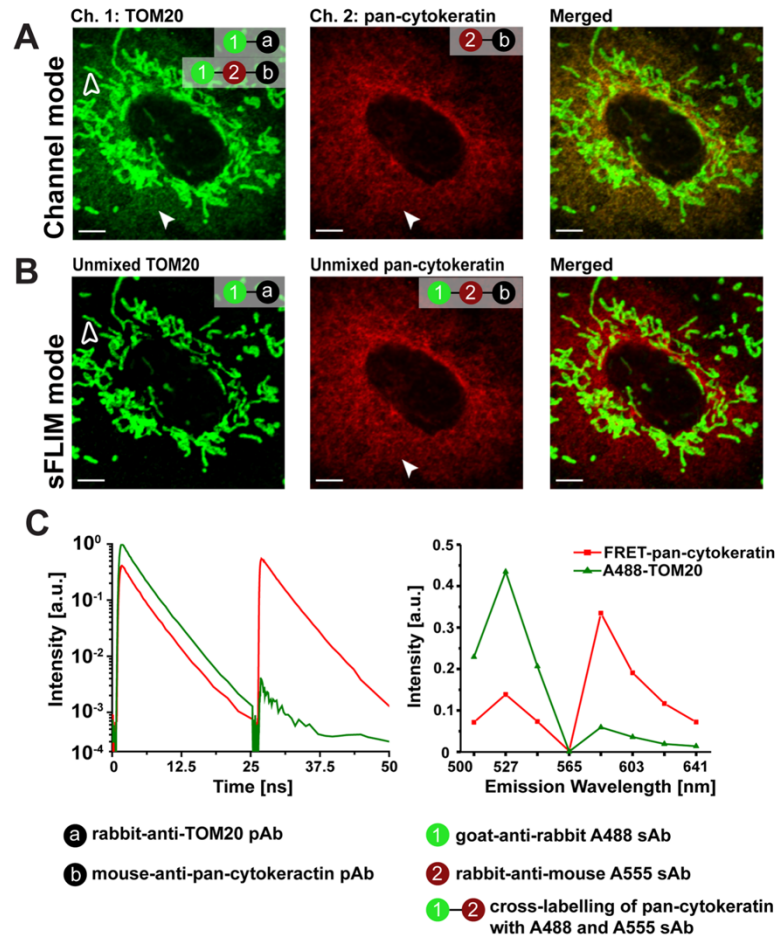


**Figure 4.** Spectral-FLIM-FRET for separation of cross-labelling in dual antigen indirect immunofluorescence. A549 cells were immunolabelled for TOM20 (with “goat-anti-rabbit Alexa488”) and pan-cytokeratin (with “rabbit-anti-mouse Alexa555”) antigen leading to single labelling of TOM20 and cross-labelling of pan-cytokeratin (arrowhead) to the TOM20 channel (open arrowhead). (A) Conventional channel mode imaging is insufficient for eliminating the attribution of pan-cytokeratin (arrowhead) to the TOM20 channel (open arrowhead). (B) The same cells were measured by spectral-FLIM. Pattern based unmixing provides pixelwise the fluorescence contributions for Alexa488 labelled TOM20 (open arrowhead) and cross-labelled pan-cytokeratin (closed arrowhead). Each labelled antigen structure now is clearly attributed to separate analysis channel. (C) Fluorescence decays (left panel) corresponding to two excitation laser pulses (485 nm and 561 nm) and emission spectra (right panel) were used as combined reference patterns for unmixing Alexa488 labelled TOM20 and FRET antibody pair labelled pan-cytokeratin (Alexa488 and Alexa555). Representative images from three independent experiments are shown; scale bars 5  $\mu$ m.

of fluorescence signals from cross-labelled pan-cytokeratin is impossible by conventional filter-based microscopy (Fig. 4A). However, by using appropriate reference patterns corresponding to each labelled antigen and a pattern-matching algorithm for quantitative estimation of fluorescence contribution of both antigens per pixel, we could precisely attribute single-labelled TOM20 and cross-labelled pan-cytokeratin into separate analysis channels (Supplementary Fig. 3 and Fig. 4B). A reference pattern is defined as a characteristic fluorescence signature of antigen labelling combining both information, emission spectra as well as time-resolved fluorescence decays. The dip in the recorded reference emission spectra is due to the use of the notch filter used to avoid detection of scattered light from 561 nm excitation wavelength. For optimal unmixing of fluorescence signals of both labelled antigens, we used reference patterns obtained from “goat-anti-rabbit Alexa488” labelled TOM20 sample, whereas pan-cytokeratin FRET reference pattern was obtained from dual antigen IMF sample (Fig. 4C, see



Material and Methods for details). A direct comparison of the resulting merged multi-colour fluorescence images obtained by channel mode (Fig. 4A, merged) and sFLIM (Fig. 4B, merged) as well as the comparison of line profiles of selected region (Supplementary Fig. 5A) clearly demonstrates the advantage gained by multi-dimensional sFLIM acquisition followed by linear-unmixing based pattern-matching data analysis.

**sFLIM-FRET enables triple antigen IMF by using just two fluorophores.** To further demonstrate the potential of sFLIM for separation of cross-labelling, triple antigen IMF for TOM20, pan-cytokeratin and golgin was performed with a combination of two species for primary AB origin (mouse, rabbit) as well as two fluorophore-tagged secondary AB (“rabbit-anti-mouse Alexa546” and “goat-anti-rabbit Alexa488”). Following the proposed labelling sequence, pan-cytokeratin was positive for “rabbit-anti-mouse Alexa546”, TOM20 for “goat-anti-rabbit Alexa488”, and golgin for “rabbit-anti-mouse Alexa546” (Supplementary Fig. 4A). This procedure inevitably led to additional cross-labelling of pan-cytokeratin with “goat-anti-rabbit Alexa488” and subsequent FRET effects between interacting fluorophore-tagged AB. This was verified by extracting the mean lifetime from the fluorescence decays obtained from sFLIM measurements of cross-labelled (FRET control) and donor only (no-FRET control) labelled pan-cytokeratin sample (Supplementary Table 1C). Data indicates a clear pan-cytokeratin related FRET effect caused by fluorophore-tagged AB cross-labelling ( $\Delta\tau_{int} = 0.67$  ns, difference between unquenched and quenched donor fluorophore intensity weighted lifetime). It is important to follow the correct labelling steps to achieve triple antigen IMF using two fluorophores, and we illustrate this in another exemplary scenario (Supplementary Fig. 4B). Next, we again demonstrate that filter-based channel mode imaging is insufficient for separating cross-labelled fluorescence signals from three labelled antigens (Fig. 5A). It can be seen that pan-cytokeratin is false-positively attributed in TOM20 and golgin channel, thereby completely covering the golgin signal. Taking advantage of multi-dimensional sFLIM followed by pattern-matching analysis, however, pixelwise quantitative separation of fluorescence contribution from all three immunolabelled antigens into different fluorescence analysis channels was possible, albeit the complexity due to spatial overlap of all antigens (Fig. 5B). The clear separation of fluorescence signal into different color channels is demonstrated very nicely in line profiles plots of selected regions in merged image (Supplementary Fig. 5B). For optimal unmixing results, reference patterns generated from single labelled TOM20 and golgin control samples were used, whereas it was appropriate to generate pan-cytokeratin reference pattern from triple antigen IMF samples (Fig. 5C). Bleed-through estimated from unmixed pan-cytokeratin channel to unmixed TOM20 and golgin channel were less than 2%. And, bleed-through of unmixed TOM20 and golgin channels into other unmixed channels were less than 1% (data not shown).

## Discussion

In this study, we present a novel imaging strategy suitable to leverage false-positive cross-labeling in IMF for precise multiple antigen detection. We describe a definitive labeling procedure and correct selection of controls as well as fluorophores serving as proper FRET pairs to perform sFLIM analysis for attribution of new fluorescence analysis channels corresponding to cross-labelled antigens. To demonstrate the power of this method, double and even triple antigen IMF was carried out by use of just two fluorophores, which would be impossible to separate by conventional channel mode imaging in cross-labelling scenarios. This advantage and precision become possible since the pattern-matching analysis of sFLIM data provides minimal bleed-through between unmixed fluorescence channels, as already demonstrated in our previous study where up to nine fluorophores were intra-cellularly separated<sup>15</sup>. Based on these findings we demonstrate herein, next to mere fluorophore separation, sFLIM allows for labelling of different cellular antigens with ABs raised in the same species.

The major advantage of this microscopic method and analysis is that IMF protocols with often well-established primary ABs can be maintained and require just adaption for the new labelling sequence of the secondary AB to get proper controls as well as efficient FRET effects on double labelled antigens. Consequently, no establishment of new IMF kits for avoiding false-positive cross-labelling is necessary, which saves time, costs and, most importantly, helps to avoid misinterpretation such as wrongly attributed co-localization or spatial distribution of cellular structures and proteins. Indeed, previous studies have already shown that it is possible to achieve double or multiple staining of target biomolecules with ABs derived from the same species. For instance, Tsurui *et al.* established a method for seven-colour analysis of immunofluorescence stained tissue with a labelling scheme consisting of monoclonal AB treated with avidin-biotin complex (ABC) in combination with seven distinct fluorophores<sup>6</sup>. Although, use of high ABC ratios allows for increased sensitivity, but at the same time bears the risk of increased non-specific background since avidin can bind to endogenous biotin in cells and tissues<sup>3</sup>. Additionally, the filter-based imaging setups used in these studies allow just for sequential excitation per dye group (blue, green, red) and data analysis requires additional dummy exposure images to remove false-positive contribution/bleed-through from shorter wavelength dye groups into red ones. In comparison, sFLIM can be carried out with simultaneous excitation due to pulse interleaved excitation (PIE) and multi-color acquisition and, even more important, provides better signal to noise ratios since both, decay and spectral information, are combined in the unmixing algorithm leading to images with minimal bleed-through and precise fluorophore channel attribution.

In another approach, researchers demonstrate the effective use of primary ABs raised in same species to visualize two antigens simultaneously<sup>4,7,8</sup>. However, these methods require an intermediate blocking step with AB F(ab) fragments for the first staining which results in higher background due to non-specific binding of blocking AB fragments, and consequently, decreased intensity of first labelling possibly due to over-blocking of AB on the first antigen<sup>4</sup>. Following a similar approach, Franzusoff *et al.* were able to demonstrate labelling of two antigens with two rabbit primary antibodies treated with “goat-anti-rabbit” and “mouse-anti-rabbit” F(ab) fragments and visualized using “rabbit-anti-goat FITC” and “rabbit-anti-mouse TRITC”, respectively<sup>9</sup>. However, a limitation of this method is that primary antibodies must be pre-treated in solution to avoid any cross-labelling between

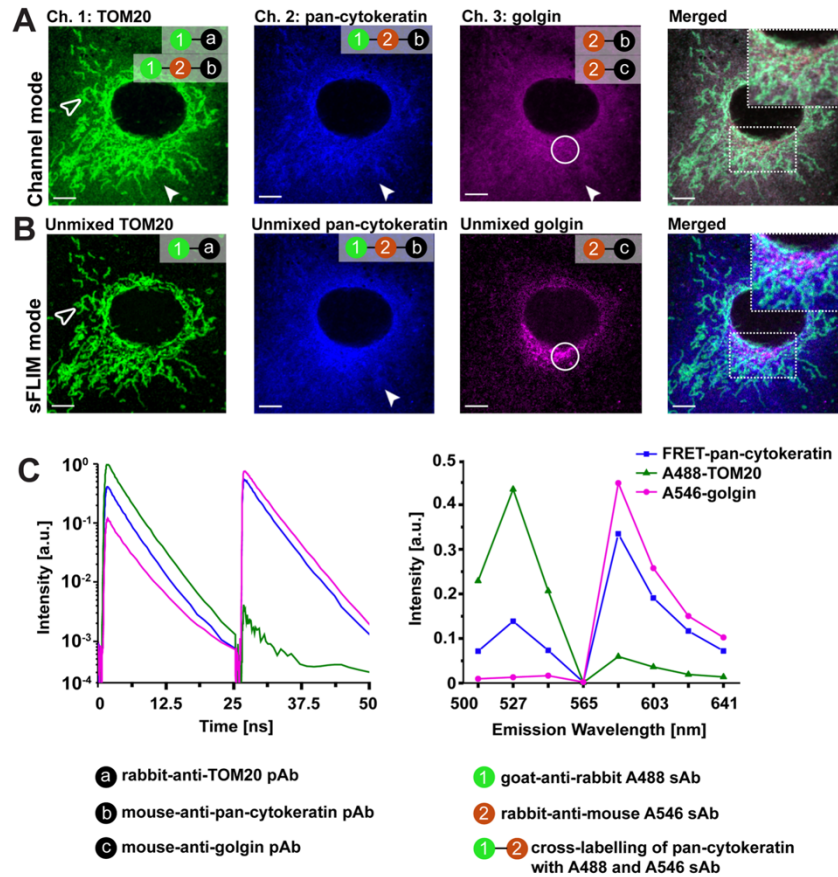


**Figure 5.** Spectral-FLIM-FRET for separation of cross-labelling in triple antigen indirect immunofluorescence. A549 cells were immunolabelled for three different cellular antigens with just two primary (mouse, rabbit) and secondary (“goat-anti-rabbit Alexa488”; “rabbit-anti-mouse Alexa546”) antibody (AB) species types. Following a sequential labelling scheme, single labelling of TOM20 (“goat-anti-rabbit Alexa488”), golgin (“rabbit-anti-mouse Alexa546”) and cross-labelling of pan-cytokeratin (“goat-anti-rabbit Alexa488”; “rabbit-anti-mouse Alexa546”) was achieved. (A) Conventional channel mode imaging was insufficient for eliminating false-positive pan-cytokeratin (closed arrowhead) in the TOM20 channel and golgin channel. (B) The spectral-FLIM data acquisition and pattern-matching analysis allows to separate the fluorescence contributions of all three antigens into independent analysis channels: Different structures (TOM20 (open arrowhead), pan-cytokeratin (closed arrowhead), golgin (open circle)) are clearly visualized with a notable false-positive suppression (compare merged images of A and B). (C) Reference patterns, combining fluorescence decay (left panel, 485 nm and 561 nm excitation laser wavelength were used) and emission spectra (right panel) information, of Alexa488 labelled TOM20, Alexa546 labelled golgin as well as FRET AB pair labelled pan-cytokeratin used by pattern-matching algorithm for unmixing of their fluorescence contribution per pixel. Representative images from three independent experiments are shown; scale bars 5  $\mu$ m.

anti-rabbit AB fragments, which probably reduces the affinity of the primary ABs for their target antigens in addition to increased sample preparation time steps (three step labelling procedure instead of typical two step IMF). In total, the labelling scheme which we propose in this study, provides a novel solution to circumvent the problem of limited variability of primary AB species for IMF studies.

Although using FLIM for FRET analysis is technically demanding, this method is still recognized as the gold standard for quantitative FRET as demonstrated in the study by Pelet *et al.*<sup>22</sup>. Similar methods such as acceptor photo-bleaching or sensitized emission would be completely insufficient to identify cross-labelled antigens precisely. In the first approach, acceptor fluorophores of the entire cell would have to be bleached to identify areas of donor fluorophores (which are hidden among none-donor fluorophores), which would at the same time destroy

the fluorescence of all acceptors (including non-cross-labelled). In the second approach, donor excitation for measuring sensitized emission would be probably useful to identify signals just in FRET positive areas, however, in a non-quantitative and spatially unprecise manner. This has a certain reason: normally, sensitized emission is used in scenarios where just FRET or non-FRET should be identified to infer a yes or no effect. However, the precise spatial separation of FRET and non-FRET fluorophores, where 'correct' and 'false-positive' cross-labelling has to be accurately distinguished, is not at all the domain of this approach. A more advanced method would be if the sensitized emission method is used in spectral mode where the donor/acceptor ratio can be measured at once. However, even spectral FRET alone is insufficient to quantitatively distinguish donor/acceptor fluorophores from non-donors/non-acceptors leading to a false attribution of fluorescence channels. Therefore, we used the time domain FLIM technique in this proof of concept study to quantify FRET effects due to cross-labelling ABs, in solution as well as in cellular IMF. FLIM was further combined with the spectral domain since the former is necessary for separating fluorophores in more complex multiplex scenarios where fluorophore emission spectra are strongly overlapping. The benefit for the unmixing results has been demonstrated in our previous study, where it was shown that separation quality decreased substantially when spectral or lifetime information for unmixing were used separately<sup>15</sup>. In total, the inherent ability of the sFLIM method to resolve fluorophores with spectroscopically similar fluorescent signatures or even FRET of cross-labelling ABs, as shown here, potentially enhances the possible number of combinations of fluorophores which could be multiplexed, imaged and visualized simultaneously. This is supported by comparable studies which likewise demonstrate that sFLIM successfully enables FRET quantitation with high accuracy<sup>23–25</sup>.

While our study provides an easy to use labelling procedure leveraging FRET effects between cross-labelling ABs for generating additional fluorescence analysis channels, it is nevertheless important to consider that the labelling sequence and AB concentrations might affect the ratio of donor to acceptor molecules on the FRET pair labelled antigen. For instance, it is expected that FRET effects will be stronger for conditions where multiple acceptor molecules are available per donor molecule. We noticed similar increased FRET effects (or larger decrease in donor fluorophore lifetime) on pan-cytokeratin which could possibly be explained by the surplus of acceptor molecules in triple antigen IMF (see Supplementary Fig. 4A). Similar effects were also reported in two independent studies, where it was shown that presence of two acceptor molecules per single donor molecule leads to significant increase in FRET effects<sup>26,27</sup>. We also noticed that stronger FRET effects lead to better separation quality of cross-labelled antigen from single labelled antigen due to significant differences in their fluorescence signatures (data not shown). Furthermore, for schematic illustration we simplified the labeling stoichiometry to 1:1 between fluorophores and Abs as well as for secondary AB to single primary AB binding. However, several fluorophore molecules and secondary ABs with an unknown exact ratio must be considered to be attached respective binding partners (see Fig. 1, Supplementary Figs. 1 and 4). This fact leads to higher stoichiometry between fluorophores and ABs and is considered to potentially stabilize FRET effects as the probability of donor or acceptor fluorophore missing on the ABs is reduced. For a deeper analysis, measurements of molecular brightness e.g. by using FCS could be performed to determine the degree of labelling by comparing brightness of single and multi-fluorophore-tagged secondary ABs. In general, the success of the labelling approach described in this study greatly depends on whether the cross-labelling fluorophore ABs are FRET compatible or not. As shown by Holzapfel *et al.*, use of Fab fragments, as opposed to full IgG molecules, will exhibit observable FRET on cross-labelled antigen, since the large size of full IgG molecules compared to Fab fragments leads to decreased interaction between donor and acceptor fluorophores<sup>14</sup>. This has to be taken into consideration. Another crucial aspect to be taken into account is the significant change in fluorescence lifetime values of fluorophore-tagged secondary ABs going from unfixed solution to fixed samples in cells of IMF (see Supplementary Table 1). This phenomenon is well known and shows again the dependency of fluorophore lifetime on the actual environment influenced by fixation, pH, mounting media, etc. In a study by Joosen *et al.*, similar findings and necessary control experiments were suggested to account for such causes and effects<sup>28</sup>. Hence, it is an important pre-requisite to perform control studies and experiments to ensure FRET interaction among interacting AB as free dyes in solution, which is indeed easy to perform. While one might be tempted to use higher AB concentration to achieve stronger FRET effects, one must find, through trial and error experiments, optimal primary and secondary AB concentrations in addition to labelling specificity and efficiency to avoid artefacts due to any non-specific background staining. The choice of labelling sequence could also affect the number of acceptor molecules per donor molecule or even no FRET labelling on target antigen at all. For example, in triple antigen IMF, performing the TOM20 labelling first will result in cross-labelling of pan-cytokeratin with "rabbit-anti-mouse Alexa546" AB which makes it difficult to separate from golgin due to their similar spectral and fluorescence decay properties.

In essence, this new microscopic approach presented herein allows researchers to use the adversity of cross-labelling artefacts in IMF to their advantage and, at the same time, provides a general solution for multiplex IMF using AB originating in the same host animal species. Thus, researchers can develop individual labelling schemes based on already well-established primary ABs combined by using various commercially available fluorophores of secondary ABs which are proper FRET pairs (e.g. Cy3/Cy5 or ATTO488/ATTO565 etc.). Taken together, an adapted IMF labelling protocol in combination with sFLIM and pattern-matching analysis serves as innovative and proper method benefitting the entire research field where AB based IMF is carried out.

## Methods

**Antibodies.** The primary AB against pan-cytokeratin and TOM20 were obtained from Santa Cruz Biotech (Germany). The anti-golgin primary AB and the Alexa Fluor® conjugated secondary AB were purchased from ThermoFisher Scientific (Germany). The "unconjugated rabbit-anti-mouse" secondary AB was from Dianova (Germany).



**Cell culture and indirect immunofluorescence labelling.** Human lung alveolar epithelial cell line A549 (ATCC, CCL-185) was cultured in Ham's F12 medium (Biochrome, Berlin, Germany) supplemented with 10% fetal calf serum at 37 °C and 5% CO<sub>2</sub>. Cells were seeded on optical coverslips. After three washes with phosphate buffered saline (PBS), cells were fixed with 3% paraformaldehyde for 15 min at room temperature followed by three times washing with PBS. Afterwards, cells were permeabilized with 1.0% Triton X100 for 15 min. After washing with PBS, cells were blocked with AB diluent (20 ml PBS 0.01 M with 0.2 g BSA and 0.01 g Tween-20) and primary AB (2 µg/ml) were incubated overnight at 4 °C. After three times washing with PBS, cells were subjected to an overnight incubation with respective secondary AB at 4 °C. Immunolabelled cells were embedded in MOWIOL for 20 min at 4 °C.

**Labelling procedures for sFLIM-FRET analysis.** Dual antigen IMF of cells for pan-cytokeratin and TOM20 with non-cross-labelling AB pair was performed with "goat-anti-mouse Alexa555" and "goat-anti-rabbit Alexa488" AB, respectively. Dual labelling of pan-cytokeratin and TOM20 with cross-labelling AB pair was performed with "rabbit-anti-mouse Alexa555" and "goat-anti-rabbit Alexa488" AB (Supplementary Fig. 1). Pan-cytokeratin cross-labelled with "unconjugated rabbit-anti-mouse" and "goat-anti-rabbit Alexa488" AB served as a zero FRET (donor-only) control sample. Additionally, single antigen IMF samples were prepared to obtain reference patterns from TOM20 labelled with "goat-anti-rabbit Alexa 488" as well as pan-cytokeratin cross-labelled with FRET AB pair ("rabbit-anti-mouse Alexa555" and "goat-anti-rabbit Alexa488").

For triple antigen IMF, cells were sequentially labelled to achieve single labelling of TOM20 with "goat-anti-rabbit Alexa488" AB and golgin with "rabbit-anti-mouse Alexa546" AB as well as cross-labelling of pan-cytokeratin with "goat-anti-rabbit Alexa488" and "rabbit-anti-mouse Alexa546" FRET AB pair (Supplementary Fig. 4A). As described above, a zero FRET (donor-only on pan-cytokeratin) as well as single antigen IMF samples were also prepared to quantify FRET effects and obtain reference patterns (for TOM20 and golgin), respectively.

**Experimental setup and measurements.** Confocal microscopy was performed on a time-resolved microscope (MicroTime 200, PicoQuant, Germany) equipped with a fast galvo scanner (FLIMbee, PicoQuant, Germany) operated by the SymPhoTime 64 software (PicoQuant, Germany). We used two lasers in PIE mode with wavelengths of 485 nm and 561 nm (LDH-D-C-485 and LDH-D-TA-560; PicoQuant, Germany) operating at 40 MHz repetition rate and an average power between 3 µW to 6 µW measured after the objective. Samples were imaged using a 100×/1.4 NA oil-immersion objective (UPlanSApo, Olympus, USA). Sample regions of 40 µm × 40 µm (512 × 512 pixels) were imaged with an acquisition time set to 300 s with pixel dwell time equal to 5 µs.

Conventional channel mode measurements were performed using 520/35 nm and 593/20 nm bandpass filters (AHF Analysentechnik AG, Germany). For triple antigen IMF intensities in three analysis channels corresponded to following combinations of PIE mode and detection bandpass filters: Ch. 1 – excitation at 485 nm wavelength, detection spectral band of 520/35 nm, Ch. 2 – excitation at 485 nm wavelength, detection spectral band of 593/20 nm and Ch. 3 – excitation at 560 nm wavelength, detection spectral band of 593/20 nm.

The sFLIM measurements were performed with a custom-built (by PicoQuant, Germany) setup added to the MicroTime 200 system (Supplementary Fig. 2). The emitted fluorescence light was guided with a multi-mode fiber to the sFLIM detection system comprising of a spectrograph, an array PMT detector as well as an 8-channel TCSPC module (HydraHarp<sup>29</sup> 400, PicoQuant, Germany). The fluorescence light was dispersed with a grating-based spectrograph (Shamrock SR-163 equipped with a SR1-GRT-0600-0500 grating, Andor Oxford Instruments, UK) and detected with a custom made (by PicoQuant, Germany) 16-channel PMT array detector module equipped with a gallium arsenide phosphide (GaAsP) cathode (Hamamatsu Photonics, Japan) and power supply. Corresponding to the 8 TCSPC channels, the system was configured to create 8 spectral channels with a width of 18.8 nm each covering in total a range from 490 nm to 640 nm. Information of each detected photon was stored in the time-tagged time-resolved<sup>30</sup> (TTTR) data format, and further processed using a custom written sFLIM pattern-matching software<sup>15</sup> written in MATLAB (MathWorks, USA). This pattern-matching based data analysis was performed on a 16-core CPU (Intel<sup>®</sup> Xeon<sup>®</sup> CPU E5-2680, clock speed of 2.7 GHz).

The higher sensitivity of GaAsP cathode PMT detection array together with the fully parallel 8-channel TCSPC unit allowed for high detection efficiency and faster acquisition speed. This was a major improvement over the previously reported sFLIM system<sup>15</sup>, where the pileup constraint due to just one TCSPC channel was a huge limitation factor precluding fast data acquisition. Furthermore, we have reduced the computation time of the sFLIM pattern-matching algorithm using a multi-core CPU from an average of 50 min per image down to 3 min (for an image of 512 × 512 pixels), equaling approximately a 16-fold increase in computation speed. Work is underway to make it even faster (less than a minute) for the method to be used and incorporated by researchers in routine experimental studies.

FCS measurements were performed using the sFLIM detection system to obtain concentrations of the dyes in aqueous solution. Dye solutions were prepared using 5 µl of each fluorescent secondary AB, "goat-anti-rabbit Alexa488", "rabbit-anti-mouse Alexa555" and "goat-anti-mouse Alexa555", with a 1:100 dilution in distilled water. FCS analysis was performed using the SymPhoTime 64 software. Atto488-carboxylic acid dye (ATTO-TEC GmbH, Germany) was used to obtain an effective dimension of the confocal volume,  $V_{\text{eff}} = 0.95 \pm 0.10$  fl with  $\kappa = 5.60 \pm 0.64$  using the literature value for diffusion coefficient<sup>31</sup>,  $D = 400 \pm 1 \mu\text{m}^2/\text{s}$  measured at 25 °C. These values were used as calibration values in FCS curve fitting analysis for all corresponding AB-dye FCS measurements. Finally, we obtained absolute concentrations of "goat-anti-rabbit Alexa488" equal to  $53 \pm 1$  nM, "rabbit-anti-mouse Alexa555" equal to  $43 \pm 1$  nM and "goat-anti-mouse Alexa555" equal to  $50 \pm 1$  nM.

**Fluorescence lifetime analysis.** Fluorescence decays obtained were fitted with a bi-exponential decay function, re-convolved with the measured instrument response function, using the SymPhoTime 64 software. The quality of the fits was judged from the post fitting residuals and by the reduced chi-square values. In this study, intensity weighted as well as amplitude weighted average lifetimes were calculated and reported for each bi-exponential fit. Lifetime values are expressed as mean  $\pm$  SD from at least three independent experiments.

**Generation of reference patterns.** Single labelled TOM20 with “goat-anti-rabbit Alexa488” and golgin with “rabbit-anti-mouse Alexa555” were imaged with the described sFLIM system to generate corresponding reference patterns, whereas the FRET AB pair labelled pan-cytokeratin reference pattern was obtained from double/triple labelled samples. The sFLIM information (combining emission spectra as well as fluorescence decays corresponding to each excitation laser line) from adequately selected groups of pixels from labelled antigen were merged to generate one reference pattern. The entire procedure requires that sample preparation as well as imaging conditions are kept similar for single and multi-antigen IMF (e.g. AB incubation time, relative laser power between the two laser lines, temperature, pixel dwell time etc.).

**Bleed-through calculation.** Bleed-through is defined as the contribution of photon counts after pattern-matching analysis from an unmixed channel into another unmixed channel. The bleed-through analysis was performed as proposed by Winter *et al.* (see “residual crosstalk calculation”, Materials and Methods)<sup>32</sup>. The calculation of pan-cytokeratin signal bleed-through into TOM20 and golgin channels was straightforward, as it was convenient to find pixel regions in the images with only a pan-cytokeratin structure. To compute the bleed-through of the TOM20 and golgin into different unmixed channels, corresponding single fluorophore-AB labelled samples were prepared for each antigen and analysed using reference patterns used during triple antigen IMF unmixing.

**Statistical analysis.** GraphPad Prism 7 (Version 7.01) software was used for statistical analysis. An unpaired two-tailed Student's *t*-test was used to determine significant changes in donor fluorophore (“goat-anti-rabbit Alexa488”) lifetime after mixing of acceptor fluorophore AB (“rabbit-anti-mouse Alexa555”). Values are expressed as mean  $\pm$  SD from at least three independent experiments and the significance level ( $\alpha$ ) of 0.05 was considered significant (Fig. 3).

#### Data availability

The data generated for triple antigen IMF and used for analysis during this study is included in this published article and its Supplementary Information files. The sFLIM software package custom written in MATLAB can be downloaded here: <https://github.com/SumeetRohilla/sFLIM>.

Received: 18 October 2019; Accepted: 17 February 2020;

Published online: 02 March 2020

#### References

- Coons, A. H., Leduc, E. H. & Connolly, J. M. Studies on antibody production. I. A method for the histochemical demonstration of specific antibody and its application to a study of the hyperimmune rabbit. *The Journal of Experimental Medicine* **102**, 49–60, <https://doi.org/10.1084/jem.102.1.49> (1955).
- Fritschy, J. M. Is my antibody-staining specific? How to deal with pitfalls of immunohistochemistry. *The European journal of neuroscience* **28**, 2365–2370, <https://doi.org/10.1111/j.1460-9568.2008.06552.x> (2008).
- Ramos-Vara, J. A. Technical aspects of immunohistochemistry. *Veterinary pathology* **42**, 405–426, <https://doi.org/10.1354/vp.42-4-405> (2005).
- Lewis, C. S. A., Gillete-Ferguson, I. & Ferguson, D. G. An indirect immunofluorescence procedure for staining the same cryosection with two mouse monoclonal primary antibodies. *Journal of Histochemistry & Cytochemistry* **41**, 1273–1278, <https://doi.org/10.1177/41.8.7687266> (1993).
- Negoescu, A. *et al.* F(ab) secondary antibodies: a general method for double immunolabeling with primary antisera from the same species. Efficiency control by chemiluminescence. *Journal of Histochemistry & Cytochemistry* **42**, 433–437, <https://doi.org/10.1177/42.3.7508473> (1994).
- Tsurui, H. *et al.* Seven-color fluorescence imaging of tissue samples based on Fourier spectroscopy and singular value decomposition. *Journal of Histochemistry & Cytochemistry* **48**, 653–662, <https://doi.org/10.1177/002215540004800509> (2000).
- Valnes, K. & Brandtzaeg, P. Comparison of paired immunofluorescence and paired immunoenzyme staining methods based on primary antisera from the same species. *Journal of Histochemistry & Cytochemistry* **30**, 518–524, <https://doi.org/10.1177/30.6.6178779> (1982).
- Wurden, S. & Homberg, U. A simple method for immunofluorescent double staining with primary antisera from the same species. *Journal of Histochemistry & Cytochemistry* **41**, 627–630, <https://doi.org/10.1177/41.4.8450202> (1993).
- Franzoso, A., Redding, K., Crosby, J., Fuller, R. S. & Schekman, R. Localization of components involved in protein transport and processing through the yeast Golgi apparatus. *The Journal of Cell Biology* **112**, 27–37, <https://doi.org/10.1083/jcb.112.1.27> (1991).
- Yaziji, H. & Barry, T. Diagnostic Immunohistochemistry: what can go wrong? *Advances in anatomic pathology* **13**, 238–246, <https://doi.org/10.1097/01.pap.0000213041.39070.2f> (2006).
- Bendayan, M. Possibilities of false immunocytochemical results generated by the use of monoclonal antibodies: the example of the anti-proinsulin antibody. *Journal of Histochemistry & Cytochemistry* **43**, 881–886, <https://doi.org/10.1177/43.9.7642961> (1995).
- Josephsen, K., Smith, C. E. & Nanci, A. Selective but nonspecific immunolabeling of enamel protein-associated compartments by a monoclonal antibody against vimentin. *Journal of Histochemistry & Cytochemistry* **47**, 1237–1245, <https://doi.org/10.1177/002215549904701003> (1999).
- Mighell, A. J., Hume, W. J. & Robinson, P. A. An overview of the complexities and subtleties of immunohistochemistry. *Oral diseases* **4**, 217–223 (1998).
- Holzappel, H. Y. & Birtwistle, M. R. Creating complex fluorophore spectra on antibodies through combinatorial labeling. *Translational science* **2** (2016).
- Niehorster, T. *et al.* Multi-target spectrally resolved fluorescence lifetime imaging microscopy. *Nature methods* **13**, 257–262, <https://doi.org/10.1038/nmeth.3740> (2016).

16. Fereidouni, F., Reitsma, K. & Gerritsen, H. C. High speed multispectral fluorescence lifetime imaging. *Optics express* **21**, 11769–11782, <https://doi.org/10.1364/oe.21.011769> (2013).
17. Popteeva, M. *et al.* Fast and simple spectral FLIM for biochemical and medical imaging. *Optics express* **23**, 23511–23525, <https://doi.org/10.1364/oe.23.023511> (2015).
18. Mansfield, J. R. Multispectral imaging: a review of its technical aspects and applications in anatomic pathology. *Veterinary pathology* **51**, 185–210, <https://doi.org/10.1177/0300985813506918> (2014).
19. Zimmermann, T., Rietdorf, J. & Pepperkok, R. Spectral imaging and its applications in live cell microscopy. *FEBS Letters* **546**, 87–92, [https://doi.org/10.1016/s0014-5793\(03\)00521-0](https://doi.org/10.1016/s0014-5793(03)00521-0) (2003).
20. Elangovan, M., Day, R. N. & Periasamy, A. Nanosecond fluorescence resonance energy transfer-fluorescence lifetime imaging microscopy to localize the protein interactions in a single living cell. *Journal of microscopy* **205**, 3–14 (2002).
21. Gratton, E., Breusegem, S., Sutin, J., Ruan, Q. & Barry, N. Fluorescence lifetime imaging for the two-photon microscope: time-domain and frequency-domain methods. *Journal of biomedical optics* **8**, 381–390, <https://doi.org/10.1117/1.1586704> (2003).
22. Pelet, S., Previte, M. J. & So, P. T. Comparing the quantification of Forster resonance energy transfer measurement accuracies based on intensity, spectral, and lifetime imaging. *Journal of biomedical optics* **11**, 34017, <https://doi.org/10.1117/1.2203664> (2006).
23. Kufcsak, A. *et al.* Time-resolved spectroscopy at 19,000 lines per second using a CMOS SPAD line array enables advanced biophotonics applications. *Optics express* **25**, 11103–11123, <https://doi.org/10.1364/oe.25.011103> (2017).
24. Poland, S. P. *et al.* A high speed multifocal multiphoton fluorescence lifetime imaging microscope for live-cell FRET imaging. *Biomedical optics express* **6**, 277–296, <https://doi.org/10.1364/boe.6.000277> (2015).
25. Strat, D. *et al.* Spectrally resolved fluorescence lifetime imaging microscopy: Forster resonant energy transfer global analysis with a one- and two-exponential donor model. *Journal of biomedical optics* **16**, 026002, <https://doi.org/10.1117/1.3533318> (2011).
26. Bunt, G. & Wouters, F. S. FRET from single to multiplexed signaling events. *Biophysical reviews* **9**, 119–129, <https://doi.org/10.1007/s12551-017-0252-z> (2017).
27. Koushik, S. V., Blank, P. S. & Vogel, S. S. Anomalous surplus energy transfer observed with multiple FRET acceptors. *PLoS one* **4**, e8031, <https://doi.org/10.1371/journal.pone.0008031> (2009).
28. Joosen, L., Hink, M. A., Gadella, T. W. J. Jr. & Goedhart, J. Effect of fixation procedures on the fluorescence lifetimes of Aequorea victoria derived fluorescent proteins. *Journal of microscopy* **256**, 166–176, <https://doi.org/10.1111/jmi.12168> (2014).
29. Wahl, M., Koberling, F., Patting, M., Rahn, H. & Erdmann, R. Time-resolved confocal fluorescence imaging and spectroscopy system with single molecule sensitivity and sub-micrometer resolution. *Current pharmaceutical biotechnology* **5**, 299–308, <https://doi.org/10.2174/1389201043376841> (2004).
30. Wahl, M., Erdmann, R., Lauritsen, K. & Rahn, H.-J. Hardware solution for continuous time-resolved burst detection of single molecules in flow. BiOS '98 International Biomedical Optics Symposium 3259, <https://doi.org/10.1117/12.307325> (1998).
31. Dertinger, T. *et al.* Two-focus fluorescence correlation spectroscopy: A new tool for accurate and absolute diffusion measurements. *ChemPhysChem: a European journal of chemical physics and physical chemistry* **8**, 433–443, <https://doi.org/10.1002/cphc.200600638> (2007).
32. Winter, F. R. *et al.* Multicolour nanoscopy of fixed and living cells with a single STED beam and hyperspectral detection. *Scientific Reports* **7**, 46492, <https://doi.org/10.1038/srep46492> (2017).

### Acknowledgements

We are grateful to Katharina Hellwig for excellent technical assistance. This study is part of the Ph.D. thesis of S.R. This project has received funding to PicoQuant Innovations GmbH from the European Union's Framework Programme for Research and Innovation Horizon 2020 (2014–2020) under the Marie Skłodowska Curie Grant Agreement No. 675332. Additionally, the work was supported by the German Research Foundation (DFG SFB-TR84) to A.C.H (B6, Z1a).

### Author contributions

S.R. performed experiments and analysed data. A.C.H provided cells and reagents. B.K., F.K., I.G. and A.C.H. coordinated and supervised the study. I.G. and S.R. contributed towards the MATLAB data analysis software. S.R., B.K. and A.C.H. interpreted the data, prepared figures and wrote the manuscript. All authors have read and approved the manuscript.

### Competing interests

The authors declare no competing interests.


### Additional information

**Supplementary information** is available for this paper at <https://doi.org/10.1038/s41598-020-60877-8>.

**Correspondence** and requests for materials should be addressed to A.C.H.

**Reprints and permissions information** is available at [www.nature.com/reprints](http://www.nature.com/reprints).

**Publisher's note** Springer Nature remains neutral with regard to jurisdictional claims in published maps and institutional affiliations.

 **Open Access** This article is licensed under a Creative Commons Attribution 4.0 International License, which permits use, sharing, adaptation, distribution and reproduction in any medium or format, as long as you give appropriate credit to the original author(s) and the source, provide a link to the Creative Commons license, and indicate if changes were made. The images or other third party material in this article are included in the article's Creative Commons license, unless indicated otherwise in a credit line to the material. If material is not included in the article's Creative Commons license and your intended use is not permitted by statutory regulation or exceeds the permitted use, you will need to obtain permission directly from the copyright holder. To view a copy of this license, visit <http://creativecommons.org/licenses/by/4.0/>.

© The Author(s) 2020

## Supplementary Information

### Multi-target immunofluorescence by separation of antibody cross-labelling via spectral-FLIM-FRET

Sumeet Rohilla<sup>1, 4</sup>, Benedikt Krämer<sup>2</sup>, Felix Koberling<sup>2</sup>, Ingo Gregor<sup>3</sup>, Andreas C. Hocke<sup>4\*</sup>

<sup>1</sup>PicoQuant Innovations GmbH, Rudower Chaussee 29 (IGZ), 12489 Berlin, Germany.

<sup>2</sup>PicoQuant GmbH, Rudower Chaussee 29 (IGZ), 12489 Berlin, Germany.

<sup>3</sup>Third Institute of Physics, Georg-August-University, Friedrich-Hund-Platz 1, 37077 Göttingen, Germany.

<sup>4</sup>Charité – Universitätsmedizin Berlin, corporate member of Freie Universität Berlin, Humboldt-Universität zu Berlin, and Berlin Institute of Health, Department of Internal Medicine/Infectious Diseases and Respiratory Medicine, Charitéplatz 1, 10117 Berlin, Germany.

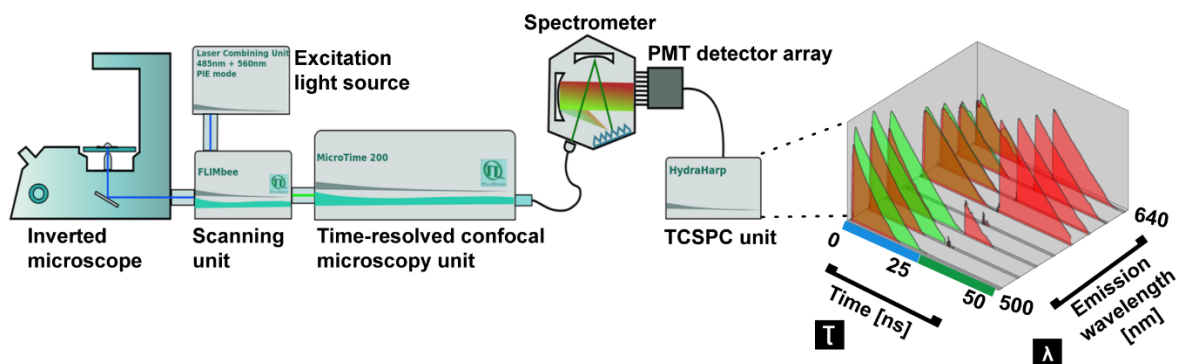
#### \*Address for correspondence

Andreas C. Hocke (MD), Charité – Universitätsmedizin Berlin, corporate member of Freie Universität Berlin, Humboldt-Universität zu Berlin, and Berlin Institute of Health, Department of Internal Medicine/Infectious Diseases and Respiratory Medicine, Charitéplatz 1, 10117 Berlin, Germany. e-mail: [andreas.hocke@charite.de](mailto:andreas.hocke@charite.de)



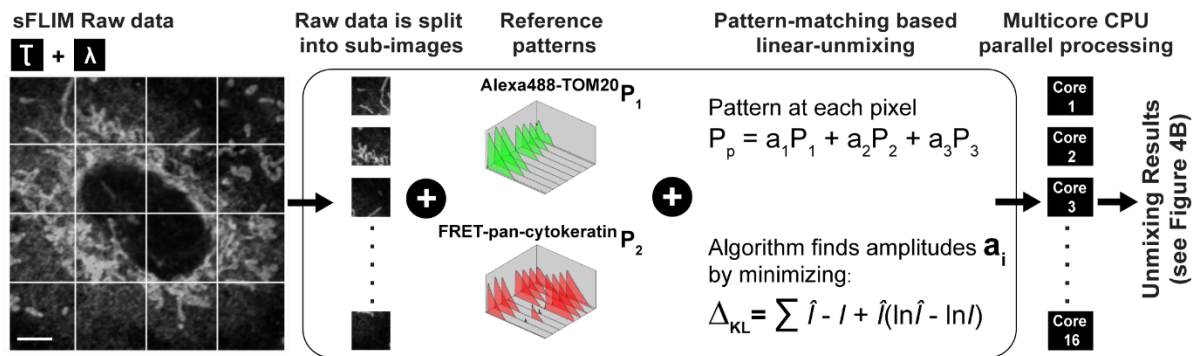


might be more than one fluorophore tagged to each secondary AB as well as more than one secondary AB attached to primary AB.



**Supplementary Figure 2. Schematic illustration of the spectral-FLIM experimental setup.**

Excitation is carried out by two lasers of wavelength 485 nm and 561 nm, operating in pulsed interleaved excitation mode, which were raster scanned over the sample. The emitted fluorescence light is spatially filtered with the confocal optics and then spectrally dispersed by a grating-based spectrometer. The light is detected with an 8-channel photomultiplier detector (PMT) array connected to an 8-channel TCSPC unit. For every image pixel we get a two dimensional spectral-FLIM data set consisting of a family of 8 photon arrival time histograms, one histogram for every spectral detection channel. Each arrival time histogram shows up to two maxima corresponding to photons being excited by a 485 nm laser pulse at about 2 ns and/or excited by a 561 nm laser pulse at about 27 ns. The setup allows for complete recording of the immunofluorescence signal, taking differences in the absorption as well as in the spectral and decay properties of the fluorescent labels into account (also called as reference pattern, see Materials and Methods for details).

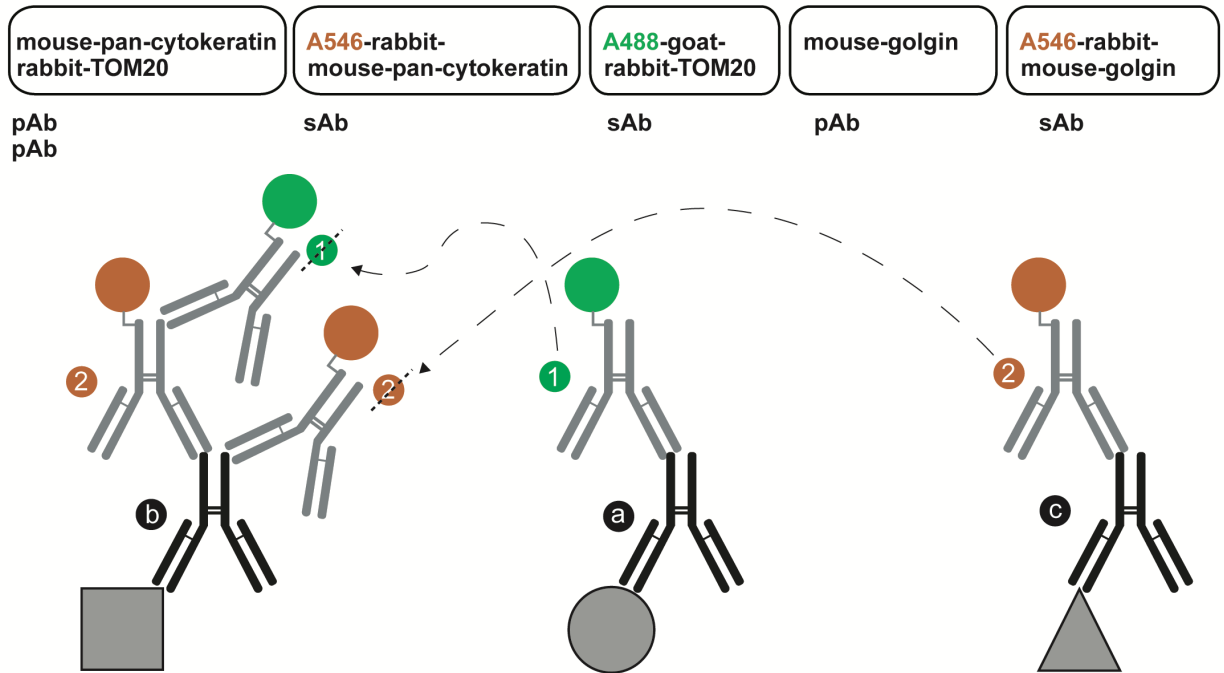


**Supplementary Figure 3. Linear-unmixing based pattern-matching approach for spectral-FLIM data analysis.**

From left to right, acquired multi-dimensional spectrally and time-resolved fluorescence lifetime imaging microscopy (spectral-FLIM or sFLIM) data is first split into sub-images. These sub-images along with a copy of reference patterns are then analysed in parallel on a multi-core CPU using a pattern-matching based linear-unmixing algorithm (see Materials and Methods for details). Here, this analysis scheme is coarsely defined as parallel batch image processing. For instance, a sFLIM image (combining emission spectra and fluorescence decay information per pixel) of size 512 x 512 pixels is then split into 16 sub-images and is processed on a 16-core CPU to finally provide the fluorescence contribution per pixel (in photon counts) corresponding to each immunolabelled antigen reference pattern.

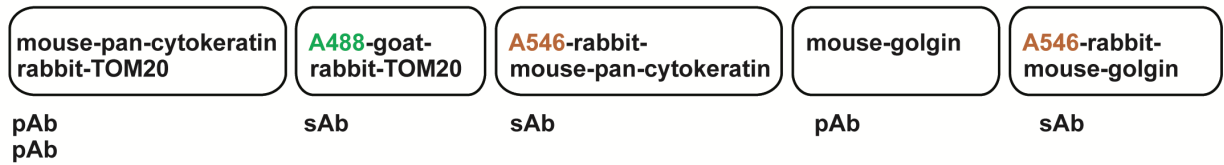
# A

Labelling sequence → (pan-cytokeratin, TOM20, golgin)



# B

Incorrect Labelling sequence → (TOM20, pan-cytokeratin, golgin)



■ pan-cytokeratin antigen

● TOM20 antigen

▲ golgin antigen

ⓐ rabbit-anti-TOM20 pAb

ⓑ mouse-anti-pan-cytokeratin pAb

ⓒ mouse-anti-golgin pAb

① goat-anti-rabbit A488 sAb

② rabbit-anti-mouse A546 sAb

① cross-labelling of pan-cytokeratin sAb with A488 sAb

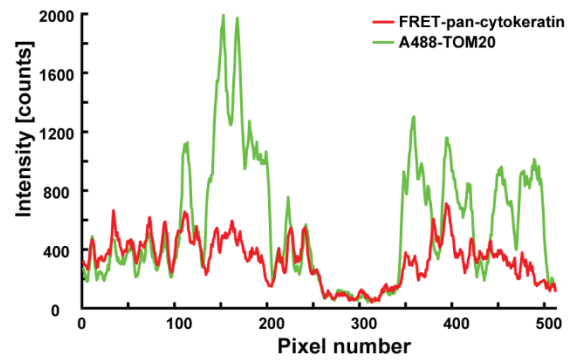
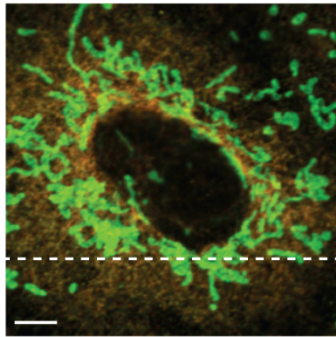
② cross-labelling of pan-cytokeratin pAb with A546 sAb

**Supplementary Figure 4. Labelling strategy for cross-labelling antibodies to achieve optimal FRET effects for triple antigen indirect immunofluorescence.**

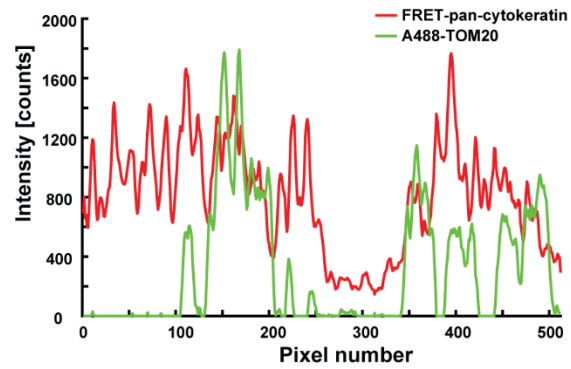
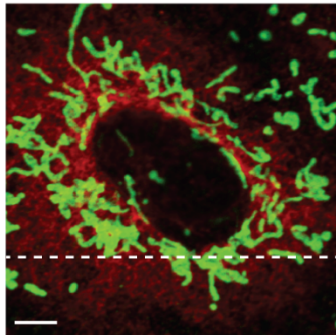
Shown are the two labelling strategies for triple antigen indirect immunofluorescence (IMF) on A549 cells and resulting cross-labelling antibody (AB) pairs on the target antigens. As a model, two secondary AB conjugates (“goat-anti-rabbit Alexa488” and “rabbit-anti-mouse Alexa546”), were used to achieve single labelling of TOM20 and golgin antigen as well as cross-labelling of pan-cytokeratin using two different labelling strategies. (A) Following the proposed sequential procedure, cells were immunolabelled for pan-cytokeratin (“rabbit-anti-mouse Alexa546”), TOM20 (“goat-anti-rabbit Alexa488”) and finally, golgin (“rabbit-anti-mouse Alexa546”). This led to labelling of TOM20 and golgin with a single type of fluorophore (Alexa488 and Alexa546, respectively), as well as cross-labelling of pan-cytokeratin with two different fluorophores (Alexa488 and Alexa546) undergoing FRET. By assigning a new fluorescence analysis channel to the FRET pair labelled pan-cytokeratin, quantitative separation of three antigens into independent analysis channels becomes possible by spectral-FLIM based data acquisition and pattern-matching based analysis. (B) The illustrated sequential IMF procedure results in labelling of TOM20 (“goat-anti-rabbit Alexa488”) and golgin (“rabbit-anti-mouse Alexa546”) as well as cross-labelling of pan-cytokeratin (“rabbit-anti-mouse Alexa546”). This incorrect labelling sequence leads to a labelling of both golgin and pan-cytokeratin antigen just with Alexa546 AB and renders it therefore difficult to quantitatively separate their fluorescence contribution into independent analysis channels. To make illustration easy to understand, stoichiometry of 1:1 between fluorophore and ABs is shown, however in reality, there could be on an average more than one fluorophore attached to secondary AB and/or more than one secondary AB tagged to primary AB.

**A**

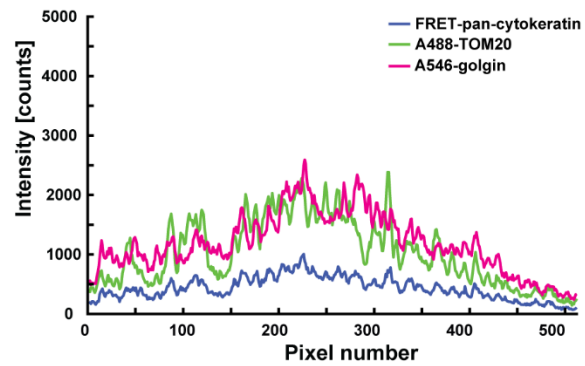
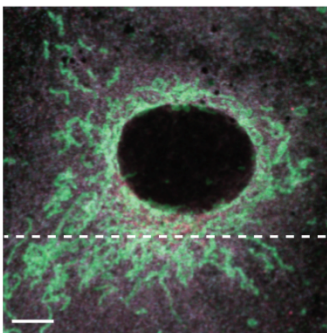
Channel mode



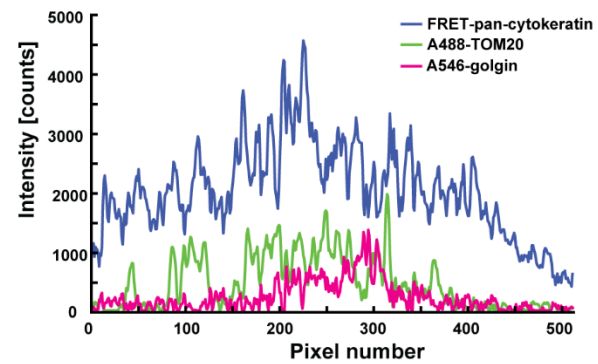
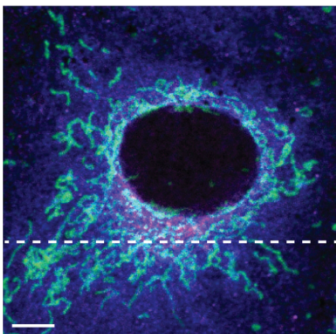
sFLIM mode

**B**

Channel mode



sFLIM mode



**Supplementary Figure 5. Spectral-FLIM FRET and pattern-matching based linear-unmixing enables proper channel attribution.** Shown are the line profiles of selected regions in merged images for channel mode and sFLIM based unmixing to demonstrate correct fluorescence attribution corresponding to (A) dual- and (B) triple- labelled samples using cross-labelling antibodies (ABs). The line profiles clearly show separation of signal into corresponding colour channels using multi-dimensional sFLIM detection and consequent data analysis using pattern-matching algorithm, which would be impossible to achieve using conventional channel mode imaging setup; scale bars 5  $\mu\text{m}$ .

## Supplementary Tables

### A

sAb-fluorophore conjugate	Type	antibody : H <sub>2</sub> O [μL]	Excitation	Emission	Lifetime	Std. dev.	Lifetime	Std. dev.
			$\lambda_{exc}$ [nm]	$\lambda_{ems}$ [nm]	$\tau_{int}$ [ns]	$\tau_{int}$ [ns]	$\tau_{amp}$ [ns]	$\tau_{amp}$ [ns]
goat-anti-rabbit Alexa488	F(ab) <sub>2</sub> IgG (H+L)	5 : 500	485	500 - 555	3.84	0.03	3.68	0.02
goat-anti-mouse Alexa555	F(ab) IgG1 (lambda L)	5 : 500	561	574 - 650	0.93	0.04	0.73	0.04
rabbit-anti-mouse Alexa555	F(ab) <sub>2</sub> IgG (H+L)	5 : 500	561	574 - 650	0.89	0.03	0.71	0.03
rabbit-anti-mouse Alexa546	F(ab) <sub>2</sub> IgG (H+L)	5 : 500	561	574 - 650	3.58	0.06	3.31	0.05
goat-anti-rabbit Alexa546	F(ab) <sub>2</sub> IgG (H+L)	5 : 500	561	574 - 650	3.49	0.02	3.33	0.03

sAb, secondary antibody

### B

Immunolabelling		Target	Excitation	Emission	Fluorophore	Lifetime	Std. dev.	Lifetime	Std. dev.
principal	cross <sup>(*)</sup>		$\lambda_{exc}$ [nm]	$\lambda_{ems}$ [nm]		$\tau_{int}$ [ns]	$\tau_{int}$ [ns]	$\tau_{amp}$ [ns]	$\tau_{amp}$ [ns]
unconjugated rabbit-anti-mouse	goat-anti-rabbit Alexa488	pan-cytokeratin	485	500 - 555	Alexa488	2.34	0.03	2.16	0.01
rabbit-anti-mouse Alexa555	goat-anti-rabbit Alexa488	pan-cytokeratin	485	500 - 555	Alexa488	1.87	0.04	1.52	0.01
goat-anti-rabbit Alexa488	-	TOM20	485	500 - 555	Alexa488	2.24	0.07	2.13	0.02
rabbit-anti-mouse Alexa555	-	pan-cytokeratin	561	574 - 650	Alexa555	1.61	0.07	1.36	0.04

### C

Immunolabelling			Target	Excitation	Emission	Fluorophore	Lifetime	Std. dev.	Lifetime	Std. dev.
principal	cross <sup>(1)</sup>	cross <sup>(2)</sup>		$\lambda_{exc}$ [nm]	$\lambda_{ems}$ [nm]		$\tau_{int}$ [ns]	$\tau_{int}$ [ns]	$\tau_{amp}$ [ns]	$\tau_{amp}$ [ns]
unconjugated rabbit-anti-mouse	goat-anti-rabbit A488	-	pan-cytokeratin	485	500 - 555	Alexa488	2.38	0.03	2.18	0.03
rabbit-anti-mouse A546	goat-anti-rabbit A488	rabbit-anti-mouse A546	pan-cytokeratin	485	500 - 555	Alexa488	1.71	0.04	1.15	0.05
goat-anti-rabbit A488	-	-	TOM20	485	500 - 555	Alexa488	2.28	0.06	2.07	0.04
rabbit-anti-mouse A546	-	-	golgin	561	574 - 650	Alexa546	2.84	0.09	2.53	0.03
rabbit-anti-mouse A546	-	-	pan-cytokeratin	561	574 - 650	Alexa546	2.79	0.05	2.54	0.03

<sup>(1)</sup> represents cross-labelling of pan-cytokeratin with Alexa488 after TOM20 principal labelling step

<sup>(2)</sup> represents cross-labelling of pan-cytokeratin with Alexa546 after golgin principal labelling step

**Supplementary Table 1. Photophysical properties of free fluorophore-tagged antibodies and immunolabelled cellular species.**

Excitation and emission maxima as well as fluorescence lifetimes were determined using the spectral-FLIM (sFLIM) system. Obtained fluorescence decays were fitted using the SymPhoTime 64 software taking into account the measured instrument response function. Intensity weighted ( $\tau_{int}$ ) as well as amplitude weighted ( $\tau_{amp}$ ) average lifetimes were calculated for each bi-exponential fit. Quantification of lifetime is given as mean  $\pm$  SD from three independent experiments. A549 cells were used for antigen indirect immunofluorescence. (A) Fluorescence lifetime values of free fluorophore-tagged secondary antibodies (AB) in aqueous solution. (B) Lifetime values obtained from measurements of A549 cells immunolabelled for TOM20 (“goat-anti-rabbit Alexa488”) and pan-cytokeratin with cross-labelling ABs (“goat-anti-rabbit Alexa488” and “rabbit-anti-mouse Alexa555”) exhibiting FRET. In addition, a “goat-anti-rabbit Alexa488” AB only labelled pan-cytokeratin sample was imaged to obtain the FRET donor only fluorophore lifetime value for FRET quantification on pan-cytokeratin. (C) Lifetime values obtained from measurements of A549 cells immunolabelled for TOM20 (“goat-anti-rabbit Alexa488”) AB and golgin with (“rabbit-anti-mouse Alex546”) as well as pan-cytokeratin with cross-labelling FRET AB pair (“goat-anti-rabbit Alexa488” and “rabbit-anti-mouse Alexa546”). Additionally, a “goat-anti-rabbit Alexa488” AB only labelled pan-cytokeratin sample was imaged to obtain donor fluorophore lifetime value for FRET quantification on pan-cytokeratin.



## **9. Curriculum Vitae**

---

My curriculum vitae does not appear in the electronic version of my paper for reasons of data protection.

## 10. List of Publications

---

No.	Year	Publication	Impact Factor
I	2020	<b>Sumeet Rohilla</b> , Bendikt Krämer, Felix Koberling, Ingo Gregor, Andreas Hocke, Multi-target immunofluorescence by separation of antibody cross-labelling via spectral-FLIM-FRET. <i>Sci Rep</i> <b>10</b> , 3820, doi:10.1038/s41598-020-60877-8 (2020).	4.011
II	2020	Michael Wahl, Tino Roehlicke, Sebastian Kulisch, <b>Sumeet Rohilla</b> , Benedikt Kraemer, and Andreas Hocke. Photon arrival time tagger with many input channels, sub-nanosecond deadtime, very high throughput, and fiber optic remote synchronization. <i>Review of Scientific Instruments</i> <b>91</b> , 013108, doi: 10.1063/1.5121412 (2020).	1.587

## ACKNOWLEDGEMENTS

---

The research work presented in this thesis would not have been possible without the incredible support and help from several incredible people.

I would like to thank my supervisor *Prof. Andreas Hocke* for his continuous guidance and support. It was always a pleasure and an immense learning process for me while discussing research ideas with him. Under his guidance, I learned a lot about microscopic methods and fluorescence imaging as well as improved my scientific writing skills. It was his meticulous attention to detail which stuck with me the most and a habit I will carry with me for ages to come.

I would like to take this opportunity to express my immense gratitude to *Dr. Benedick Krämer* and *Dr. Felix Koberling* for giving me so much of their continuous attention, technical training, and time to discuss my thesis progress whenever I demanded. In particular, I thank them for sharing their utter positivity, stimulating discussions and good company in times of dire need. Additionally, I thank my colleagues at PicoQuant - *Paja Reisch*, *Dr. Olaf Schulz*, *Dr. Evangelos Siskamis* and *Leonard Bedau* for providing memorable moments and animated crazy but feasible scientific advice in lab as well as work space. No amount of words can suffice, but I will still try! I am highly indebted to *Katharina Hellwig* for her prompt and swift technical assistance with sample preparation. Without her help, this research work would not have reached to such fruitful ends. By helping me with the administration work, she made my life easier enabling me to focus solely on research ideas. I highly appreciate her professional attitude and advice during personal conversations. I will cherish all the moments spent during my time at Charité.

I would also like to thank the BITMAP consortium for providing stimulating workshops and cross-disciplinary discussions environment.

Last, but the most important, I would like to thank my family and friends for their continuing love and support throughout my academic career.